Theory of charge-density-wave dynamics

J. R. Tucker, W. G. Lyons, and G. Gammie
Department of Electrical and Computer Engineering, Coordinated Science Laboratory, and Materials Research Laboratory, University of Illinois at Urbana-Champaign, Urbana, Illinois 61801
(Received 21 September 1987; revised manuscript received 21 December 1987)

A theoretical model is developed to describe the polarization and depinning of charge-density waves (CDW's) in the inorganic linear-chain compounds which exhibit Fröhlich sliding conduction. Each individual impurity within the crystal is assumed to pin the CDW phase very strongly at the impurity site, and dc CDW motion is made possible only by phase slip. Simple estimates are obtained for most observed properties of sliding CDW systems with use of a three-dimensional Ginzburg-Landau analysis. These predictions are found to be in excellent quantitative agreement with available experimental data characterizing virtually every aspect of CDW dynamics.

I. INTRODUCTION

Charge-density-wave (CDW) motion in quasi-one-dimensional metals has been studied intensively since 1976, when Monceau *et al.*[1] first observed the dramatic non-Ohmic behavior of $NbSe_3$. They found that the dc conductance below both Peierls transitions at $T_1=145$ K and at $T_2=59$ K could be described by the expression

$$\sigma(E,T)=\sigma_a(T)+\sigma_b(T)\exp[-E_0(T)/E]\ . \quad (1.1)$$

The functional form of the nonlinear term suggested the possibility of Zener tunneling across an energy gap, analogous to the mechanism of reverse breakdown in semiconductor p-n junctions. The estimated magnitude of this tunneling gap, however, was about 3 orders of magnitude smaller than the Peierls gap for normal quasiparticle excitations, and about 2 orders of magnitude smaller than k_BT at their experimental temperatures.

Fleming and Grimes[2] subsequently demonstrated that the nonlinear conduction sets in only for electric fields greater than a threshold value E_T. They also showed that "narrow-band noise" is observed in this region with a fundamental frequency that increases along with the non-Ohmic current. These observations were interpreted as direct evidence for CDW motion, supported by x-ray experiments[3] which showed that the CDW is not destroyed in the presence of an electric field. Experimental data of Fleming[4] illustrating the differential resistivity of $NbSe_3$ for both CDW transitions are reproduced in Fig. 1. The solid lines are fits to an expression similar to Eq. (1.1) that incorporates the dc threshold field E_T within the nonlinear term.

A strongly frequency-dependent ac conductivity was first observed by Ong and Monceau[5] in $NbSe_3$. The detailed frequency dependence was subsequently characterized by Loncor and Portis,[6] by Grüner *et al.*,[7] and by Gill,[8] who found that the observed behavior could be qualitatively characterized in terms of an overdamped oscillator. Simple theoretical models were then put forward by Grüner *et al.*[9] and by Monceau *et al.*[10] which described the general features of the observed CDW dynamics as overdamped motion of a single particle in a periodic sinusoidal pinning potential.

Meanwhile, Lee and Rice[11] interpreted CDW dynamics using Ginzburg-Landau theory, following earlier work by Fukuyama and Lee.[12] Their analysis of strong and weak impurity pinning eventually came to serve as a basis for all subsequent theoretical efforts.

Bardeen[13,14] had been the first to interpret the non-Ohmic behavior of $NbSe_3$ in terms of Fröhlich[15] sliding conduction due to CDW motion. In 1979, he resurrected the idea of Zener-type tunneling across a very small energy gap at the Fermi surface.[16] This "pinning gap" was supposed to occur in the collective excitation spectrum of the CDW, due to its weak interaction with large numbers of impurities within a phase-coherent domain. In the following year,[17] he applied photon-assisted tunneling theory, which had been highly developed[18] to describe millimeter-wave superconductor mixers, to accurately fit experimental ac-conductivity data on $NbSe_3$, using only the predicted Zener form for the dc I-V curve. The tunneling hypothesis was subsequently pursued by our own group, working in collaboration with Bardeen, over the next several years. A wide range of mixing and harmonic-generation experiments were performed in order to characterize the nonlinear ac response of TaS_3 and $NbSe_3$, and the results were found to be in reasonably good agreement with a modified version of the tunneling model.[19,20]

An alternative classical theory of CDW dynamics was proposed by Sneddon, Cross, and Fisher.[21] Their model regarded the CDW as a charged and deformable "rubber sheet," moving over randomly scattered periodic potentials located at the impurity sites. This approach was developed and extended by Klemm and Schrieffer,[22] Fisher,[23] Sneddon,[24] subsequently by many others. The mathematical complexity of these models, however, has led to very few firm predictions that could be tested against experiment. A computer simulation in one dimension was constructed by Littlewood[25] in order to illustrate many salient features of the classical model of deformable CDW's, and recently this simulation was used by Coppersmith and Littlewood[26] to predict the effects of

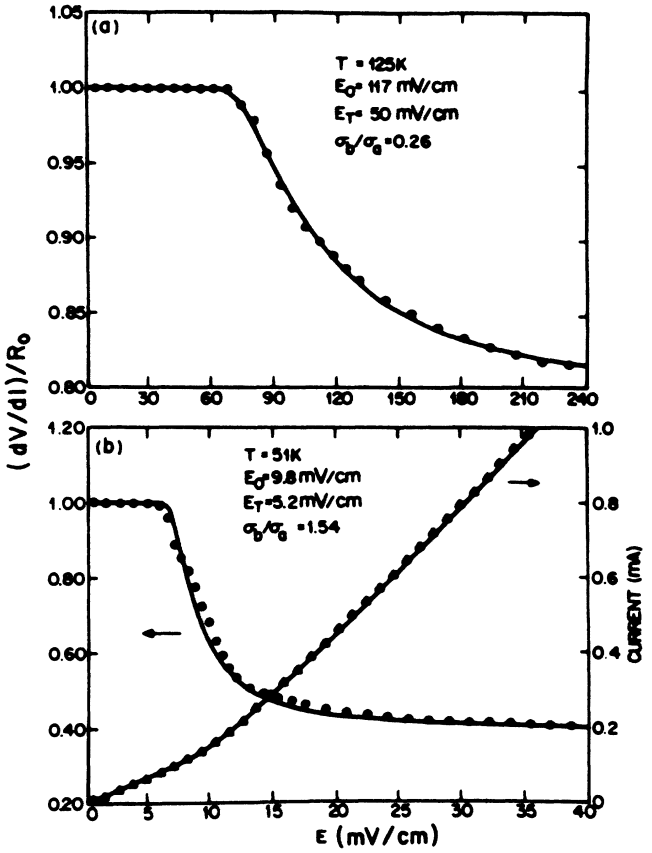

FIG. 1. Normalized differential resistance for (a) the upper and (b) the lower CDW states of $NbSe_3$. A threshold field E_T for the onset of nonlinear conduction is clearly observed. Solid lines are fits to an empirical expression $\sigma_a+\sigma_b(1-E_T/E)\exp[-E_0/(E-E_T)]$ using the indicated parameters. Reproduced from Fleming (Ref. 4).

ac-dc interference and mode locking within this framework.

The predictions of Coppersmith and Littlewood appeared to be in rough general agreement with the experimental data[27–29] on ac-dc interference that was available to them at the time. Our own recent studies of current oscillation and ac-dc interference phenomena[30] in $NbSe_3$, however, produced data of much higher quality that directly contradicts[31] all of their qualitative conclusions. This dramatic disagreement between our experimental findings and the predictions of Coppersmith and Littlewood results, we believe, from a critical difficulty of the underlying Sneddon, Cross, and Fisher model.

In their theory, the CDW phase continuously deforms as it moves over the randomly distributed weak impurities in order to reduce its net pinning energy. The maximum dc drift frequency ω_d at which the CDW can quasistatically optimize its phase configuration is therefore approximately equal to the dielectric relaxation frequency ω_0, which is readily measured to be ~ 10 MHz in $NbSe_3$. At higher drift frequencies, the CDW does not have sufficient time to relax over a static phase correlation length during one cycle of the dc motion. The effect of the periodic pinning potential (but not the dissipation due to short-wavelength distortions) is therefore predicted to decrease rapidly and become negligible for $\omega_d \gg \omega_0$. The saturation that we observe in the magnitude of the current oscillations at high dc fields, together with complete ac-dc mode locking at frequencies in excess of 300 MHz, thus appears to completely invalidate the most basic assumption of this phase-only model.

This conclusion has led us to explore a classical theory for CDW dynamics in which the pinning to individual impurities is assumed to be so strong that dc motion can proceed only by phase slip. In contrast to phase-only models, the process of amplitude collapse and phase slip necessarily preserves the effects of the periodic pinning potential to arbitrarily high dc fields and drift frequencies. Furthermore, we have found that this theory produces very simple predictions which are in excellent quantitative agreement with experimental data on virtually every aspect of CDW dynamics. The nature of this agreement is already so extensive that we are confident that the basic ideas must be fundamentally correct, although much work remains to be done.

In this paper, we will describe our theoretical model based on strong pinning and phase slip, and illustrate its predictions with experimental data taken from many sources. No effort has been made to find data which compares particularly favorably with the theory, and we have also invested very little energy in "fine tuning" our approximations and parameter estimates in order to optimize the agreement with experiment. While many refinements suggest themselves, those improvements will be deferred to a later date. Many of the parameter estimates and some of the experimental data that we shall use are taken from the excellent review articles by Grüner and Zettl[32] and by Monceau.[33]

II. STRONG PINNING

In this section, we shall reexamine the simple free-energy arguments of Lee and Rice[11] to reach the following important conclusions.

(1) Strong pinning of the CDW phase requires only a small interaction energy in excess of $\Delta/4\sim 10^{-2}$ eV at each impurity site, where 2Δ represents the Peierls-energy gap.

(2) Phase gradients near a strong-pinning site are largely confined to a very tiny region surrounding the individual impurity. Outside these regions, the average CDW phase $\bar{\phi}$ will remain correlated over volumes much larger than the mean volume n_i^{-1} associated with a single impurity.

(3) An individual impurity does not strongly pin the phase on neighboring chains, so that longitudinal CDW displacements will be correlated over a distance comparable to the average spacing between consecutive impurities along any single chain.

The picture of strong impurity pinning developed here differs greatly from the conventional wisdom. The Lee and Rice analysis has universally been interpreted as implying that the phase-coherent volume should be the in-

verse impurity concentration n_i^{-1} for strong pinning, and that the CDW phase will be smoothly interpolated between its pinned values at the various strong-pinning sites. We believe that this view is demonstrably incorrect, and that this error has thus far precluded a correct theoretical interpretation of CDW dynamics.

Lee and Rice[11] presented an analysis of CDW pinning based upon a three-dimensional Ginzburg-Landau expansion for the free energy:

$$F=f_0\int d^3r\left[-t\,|\psi|^2+\tfrac{1}{2}|\psi|^4+\xi_x^2\left|\frac{\partial\psi}{\partial x}\right|^2+\xi_y^2\left|\frac{\partial\psi}{\partial y}\right|^2+\xi_z^2\left|\frac{\partial\psi}{\partial z}\right|^2\right]. \tag{2.1}$$

Here $t=(T_p-T)/T_p$ is the reduced temperature, and the magnitude of the order parameter has been normalized so that $|\psi|\to 1$ for $T\ll T_p$. The CDW condensation energy is then $f_0/2$ per unit volume at low temperatures, and the amplitude coherence lengths ξ_x,ξ_y,ξ_z represent the distance scales over which spatial variation of the order parameter costs the entire condensation energy.

Conduction along the chain direction can be represented in terms of a tight-binding band:

$$\varepsilon(k)=-\frac{W_\parallel}{2}\cos(ka_\parallel),\quad -\frac{\pi}{a_\parallel}<k<\frac{\pi}{a_\parallel}. \tag{2.2}$$

Bandwidths for several sliding CDW materials are inferred to lie in the range $W_\parallel\approx 1$–4 eV, based on spin-susceptibility and thermopower measurements.[32] The bands are nearly $\frac{1}{4}$-filled in all materials, so that $k_F\approx\pi/4a_\parallel$ with an average spacing $a_\parallel\approx 3.4$ Å between metal atoms along the chain direction. Accordingly, the Fermi velocity is given by

$$v_F=W_\parallel a_\parallel/2\sqrt{2}\hbar\approx(1.8\times 10^7\ \mathrm{cm\,s^{-1}})W_\parallel(\mathrm{eV}) \tag{2.3}$$

and the band mass is

$$m_b=\hbar k_F/v_F\approx\frac{1.4}{W_\parallel(\mathrm{eV})}m_e, \tag{2.4}$$

where m_e represents the free-electron mass.

When the Peierls-energy gap 2Δ is opened, the $T=0$ condensation energy becomes

$$\tfrac{1}{2}f_0=\tfrac{1}{4}N(0)\Delta^2\approx\frac{\Delta^2}{2\pi\hbar v_F A_0}. \tag{2.5}$$

Here A_0 is the cross-sectional area per CDW chain, and we have used the one-dimensional density of states $N(0)=2/\pi\hbar v_F$ at the Fermi surface.

The amplitude coherence length along the chain direction is given by the BCS expression

$$\xi_\parallel=\hbar v_F/\pi\Delta\approx(0.38\ \text{Å})W_\parallel/\Delta. \tag{2.6}$$

For most sliding CDW materials, the gap parameter lies in the range $\Delta\approx 0.04$–0.12 eV, so that for $W_\parallel\approx 1$–4 eV this gives $\xi_\parallel\approx 10$ Å. The transverse coherence lengths are not known, but an estimate can be made based upon the reduction of the transition temperature T_p below its mean-field value, $T_p^{\mathrm{MF}}=\Delta/1.76k_B$, due to the quasi-one-dimensional nature of the band structure. This calculation, whose details are summarized in Appendix A, yields an average value

$$\xi_\perp\approx 0.08\xi_\parallel \tag{2.7}$$

approximately independent of material. It is important to note that $\xi_\perp\approx 1$ Å, and will thus in all cases be much smaller than the transverse spacing between CDW chains.

TABLE I. Parameter estimates for the upper $NbSe_3$, orthorhombic TaS_3, and $(TaSe_4)_2I$ CDW systems used in generating numerical predictions from the theory. The value for Δ in $NbSe_3$ has been estimated by scaling from the o-TaS_3 gap according to the ratio of the transition temperatures. The values for $W_\parallel$ are based on scaling a rough experimental estimate for $NbSe_3$ according to the ratio of the Peierls gaps. The asterisks are explained in the text.

	$(NbSe_3)^I$	o-TaS_3	$(TaSe_4)_2I$
n (10^{21} cm^{-3})		6.5[a]	3.2[a]
Δ (eV)	3.9×10^{-2} *	6.0×10^{-2}[b]	0.12[b]
M_F/m_e	300[c]	10^3[d]	10^4[e]
$W_\parallel$ (eV)	1.8*	2.8*	5.5*

[a] Reference 32.
[b] Reference 33.
[c] Reference 34.
[d] Reference 35.
[e] Reference 36.

In the following sections, we shall make detailed comparisons with experimental data primarily for the upper $(NbSe_3)^I$ transition, orthorhombic TaS_3, and $(TaSe_4)_2I$. The necessary parameters are listed in Table I, together with their sources. An asterisk denotes quantities that have not been accurately measured, and we have chosen these particular values as reasonable estimates. The Peierls gap for the $(NbSe_3)^I$ CDW cannot be inferred from temperature-dependent resistivity data, since this material does not undergo a complete metal-insulator transition. The value of Δ listed for $(NbSe_3)^I$ in Table I has simply been scaled from the o-TaS_3 result by the ratio of the transition temperatures. Experimental estimates for the longitudinal bandwidth of $NbSe_3$ have yielded $W_\parallel\approx 1.2$ eV on the basis of room-temperature spin susceptibility,[37] and a calculated value[38] of $W_\parallel\approx 2.8$ eV based on the measured thermopower.[39] The estimate $W_\parallel\approx 1.8$ eV is adopted here, and the values listed for o-TaS_3 and $(TaSe_4)_2I$ have been scaled up by the ratios of their Peierls gaps. Simple mean-field theories predict the relation $\Delta\approx 2W_\parallel\exp(-1/\bar{\lambda})$, so that this procedure is equivalent to assuming a uniform electron-phonon coupling constant $\bar{\lambda}$. The result is that we have only a crude estimate for $W_\parallel$ in these materials. Fortunately, most of the quantitative results obtained in the following sections depend, if at all, only on the square root of the bandwidth.

Lee and Rice chose z as the chain axis and rescaled the transverse dimensions in Eq. (2.1) according to $x'=(\xi_z/\xi_x)x$ and $y'=(\xi_z/\xi_y)y$, so that the gradient term could be represented as in an isotropic system:

$$F(\nabla\psi)=f_0(\xi_x\xi_y/\xi_z^2)\int dx'\int dy'\int dz\,\xi_z^2\,|\nabla\psi|^2 . \quad (2.8)$$

For strong pinning, the CDW phase is constrained to an optimal value ϕ_0^i at each pinning site. Considering only a single impurity, they estimated the energy needed to interpolate the phase between ϕ_0 at that one strong-pinning site and a fixed value $\bar{\phi}$ at infinity. Replacing $|\nabla\psi| \rightarrow |\bar{\phi}-\phi_0|/L$ in Eq. (2.8), the energy cost is seen to grow linearly with the length scale L within their three-dimensional model:

$$F(\nabla\psi)\approx f_0\xi_x\xi_y\left[\frac{(\bar{\phi}-\phi_0)^2}{L^2}\right]L^3 . \quad (2.9)$$

According to this argument, the system will seek to make L as small as possible. In this limit $L\approx\xi_z$, since more rapid phase gradients would reduce the magnitude of the order parameter and sacrifice the condensation energy. Also, the replacement $\xi_x\xi_y \rightarrow A_0$ should be made in Eq. (2.9) whenever the transverse coherence lengths are smaller than the interchain spacing. Lee and Rice thus estimate the pinning energy due to a single strong impurity as

$$E_{\rm pin}^{\rm LR}(\bar{\phi}-\phi_0)\approx f_0 A_0\xi_\parallel(\bar{\phi}-\phi_0)^2 . \quad (2.10)$$

We know from Eq. (2.7) that the transverse coherence lengths are indeed much smaller than the interchain spacing. Under these conditions, the system can actually do somewhat better in minimizing its gradient energy than the Lee-Rice estimate suggests. Here we paraphrase their argument, but now consider a volume with length L and area A:

$$F(\nabla\psi)\approx f_0 AL\left[2\xi_\perp^2\left|\frac{\partial\bar{\phi}}{\partial x_\perp}\right|^2+\xi_\parallel^2\left|\frac{\partial\bar{\phi}}{\partial x_\parallel}\right|^2\right]$$
$$\approx f_0\left[2\xi_\perp^2 L+\frac{A\xi_\parallel^2}{L}\right](\bar{\phi}-\phi_0)^2 , \quad (2.11)$$

where we have taken $|\partial\bar{\phi}/\partial x_\perp|\approx|\bar{\phi}-\phi_0|/\sqrt{A}$ and $|\partial\bar{\phi}/\partial x_\parallel|\approx|\bar{\phi}-\phi_0|/L$. This expression will again be minimized for the smallest possible area A_0, the area of a single chain, since transverse phase variations on a scale smaller than the interchain spacing would make no physical sense. Minimizing with respect to L, however, yields a larger optimum value,

$$L_0\approx\xi_\parallel(A_0/2\xi_\perp^2)^{1/2} , \quad (2.12)$$

and a lower pinning energy,

$$E_{\rm pin}(\bar{\phi}-\phi_0)\approx\left[\frac{8\xi_\perp^2}{A_0}\right]^{1/2} f_0 A_0\xi_\parallel(\bar{\phi}-\phi_0)^2 . \quad (2.13)$$

The reduction from the original Lee-Rice estimate is contained within the square-root factor. Using a representative value $\xi_\perp\approx 0.8$ Å, together with a cross-sectional area $A_0\approx 70$ Å^2 per CDW chain, gives

$$\left[\frac{8\xi_\perp^2}{A_0}\right]^{1/2}\approx\tfrac{1}{4} . \quad (2.14)$$

The value $A_0\approx 70$ Å^2 that we have used here deserves some comment. For $NbSe_3$, the unit-cell cross section is 15.6×10.0 Å^2 and contains six chains. However, these six may be grouped into three separate two-chain sets, and, roughly speaking, only one of these two-chain sets is associated with each CDW transition. The cross-sectional area per CDW chain for either transition is thus ≈ 80 Å^2 An identical estimate can be made for monoclinic TaS_3, which is isostructural to $NbSe_3$. For orthorhombic TaS_3, the detailed crystal structure is unknown, but we might guess that the area per CDW chain could be as small as half the corresponding value in $NbSe_3$, or ≈ 40 Å^2, on the basis that only one CDW transition takes place in which all of the conducting chains participate. For $(TaSe_4)_2I$ the $(9.5$ Å$)^2$ unit cell contains two equivalent chains, so that the area per chain is ≈ 45 Å^2. To simplify our analysis, we shall adopt the representative value $A_0\approx 70$ Å^2 for all materials.

The result of Eq. (2.13) may be combined with Eqs. (2.5), (2.6), and (2.14) to yield a quantitative estimate for the pinning energy due to a single strong impurity:

$$E_{\rm pin}(\bar{\phi}-\phi_0)\approx\frac{\Delta}{4\pi^2}(\bar{\phi}-\phi_0)^2 . \quad (2.15)$$

In order to dictate the maximum phase adjustment of π, the energy gain from optimizing the phase to ϕ_0 at the impurity site must be larger than $\Delta/4\sim 10^{-2}$ eV. On this basis, we expect that most types of impurities (and defects) should act as strong-pinning centers. It is important to note that, according to this analysis, the CDW phase will be distorted from its global average $\bar{\phi}$ only within a very tiny region surrounding the strong-pinning site. The distance over which the phase is adjusted between $\bar{\phi}$ and ϕ_0 along the chain direction may be estimated from Eq. (2.12) as

$$L_0\approx 75 \text{ Å} . \quad (2.16)$$

The transverse phase variations, as we have seen, are effectively confined to the particular chain which contains the impurity.

Thus far, we have considered only the problem of a single strong-pinning center embedded within an infinite CDW system whose global phase $\bar{\phi}$ is determined at infinity. The problem of physical interest, however, concerns the behavior expected in the presence of many such impurities that are randomly distributed throughout the system. It will prove most convenient to characterize an impurity concentration n_i per unit volume by the average spacing $\bar{L}$ between consecutive impurities along any individual chain:

$$\bar{L}=\frac{1}{n_i A_0}=\frac{10^6}{n_i(\text{ppm})}a_\parallel . \quad (2.17)$$

For all sliding CDW materials $a_\parallel\approx 3.4$ Å, so that a typical value $\bar{L}\approx 1$ μm corresponds to $n_i\approx 340$ ppm.

In the presence of many strong impurities, we might at first imagine the CDW phase to be separately adjusted between its global average $\bar{\phi}$ and the pinned values ϕ_0^i at each impurity site, independently for every strong-pinning center. Were the system to do this, the average phase $\bar{\phi}$ would remain correlated over infinite distances,

and the energy cost would be given by Eq. (2.15) for each impurity.

On the other hand, we might imagine that when many strong-pinning centers are present, the CDW phase would be smoothly interpolated between its values ϕ_0^i on adjacent sites over a volume n_i^{-1} surrounding each impurity. The elastic energy required for this interpolation can be estimated by returning to Eq. (2.11) and constraining the volume AL of the phase adjustment to equal $A_0\bar{L}$, the volume of a single impurity. This calculation is carried out in Appendix B. The result is most simply presented in terms of the ratio between the elastic energy needed for a smooth interpolation and the pinning energy we computed previously for local independent phase adjustments to a constant global $\bar{\phi}$:

$$\frac{E_{\rm elast}}{E_{\rm pin}} \approx 4.9[\bar{L}(\mu{\rm m})]^{1/3} . \tag{2.18}$$

Were the system to smoothly interpolate the phase between strong-pinning sites, the phase correlation length along the chain direction would be given by

$$L_{\rm min} \approx (500\ \text{Å})[\bar{L}(\mu{\rm m})]^{1/3} . \tag{2.19}$$

The actual equilibrium phase distribution will represent some compromise between the two extremes that we have outlined here. On the basis of Eq. (2.18), we expect that the energy $E_{\rm pin}$ needed for local individual phase adjustments to a constant average $\bar{\phi}$ will be substantially smaller than $E_{\rm elast}$ required for a smooth interpolation between each strong-pinning site, so long as $\bar{L} \gg 0.01$ μm or $n_i \ll 3.5\%$. Unless the impurity concentration is very high, most of the phase adjustment should take place within a tiny volume centered on each pinning site, and the average phase $\bar{\phi}$ should remain correlated over volumes larger than that of a single impurity.

In the range of dilute impurity concentrations $\bar{L} \sim 1$ μm ($n_i \sim 340$ ppm) present in nominally "pure" CDW crystals, individual localized phase adjustments to a constant $\bar{\phi}$ cost far less gradient energy, by a factor of ~ 5, than a smooth interpolation of the phase between the impurity sites. Under these conditions, $\bar{\phi}$ will be approximately constant on a volume scale much greater than n_i^{-1}. This *average* CDW phase $\bar{\phi}$ is therefore only weakly pinned by the individual impurities, and its value will be optimized to fluctuations in the total pinning energy over relatively large phase-coherent regions. We might, therefore, seek to estimate the large-scale phase-coherence properties of the system by means of the following argument. If the average phase $\bar{\phi}(r)$ is adjusted over a volume containing N_i impurities, then the value of $\bar{\phi}$ within this region can be optimized to fluctuations in the total pinning potential to gain an energy $\sim (N_i)^{1/2} E_{\rm pin}$. The elastic energy that this costs may be obtained from Appendix B by multiplying the right-hand side of Eq. (2.18) by $N_i^{1/3}$. Equating these two expressions then leads to the result $N_i \sim 10^4[\bar{L}(\mu{\rm m})]^2$. This value is enormous. It is probably too large because, for one thing, there is some small adjustment of $\bar{\phi}(r)$ toward the optimum value ϕ_0^i at each impurity site even when $\bar{L} \sim 1$ μm. Furthermore, the above estimate is unreliable, since it requires raising the numerical factor in Eq. (2.18) to the sixth power: $(4.9)^6 \approx 10^4$. The large-scale phase correlation properties of the true equilibrium ground state are thus apparently beyond the reach of our simple arguments.

On the other hand, we are usually less interested in the properties of the equilibrium ground state than in the volume over which motion of the CDW phase will remain correlated when an external electric field is applied. Since most of the phase adjustement between the average $\bar{\phi}(r)$ and the pinned value ϕ_0^i at any impurity site takes place over a very tiny region that is effectively confined to one chain, longitudinal displacements in the phase should be correlated over a distance comparable to $\bar{L}$, the average spacing between impurities. Imagine first that each segment lying between two impurities on every chain is polarized independently in the presence of an electric field. The average distance over which CDW motion would be correlated in this case is clearly $\bar{L}$. When transverse coupling is included, this correlation distance should be reduced to the extent that an individual impurity is able to effectively pin the phase on adjacent chains. Because we estimate that the transverse phase variations associated with each individual strong-pinning site are largely confined to a single chain, we expect that CDW motion will remain correlated over distances comparable to $\bar{L}$. Similarly, we expect that motion of the average phase $\bar{\phi}(r)$ will remain correlated across the chains over dimensions at least as large as the nearest-neighbor distance between impurities in the transverse direction, approximately $(\bar{L}/a_{\parallel})^{1/3} A_0^{1/2}$.

Fung and Steeds[40] have estimated the phase correlation properties of $NbSe_3$ on the upper CDW transition by analyzing the time-dependent "twinkling" seen in their superlattice dark-field electron-microscope images. The length of the apparent domains is $L \approx 2$ μm along the chain axis. In the following section, we shall use our model to infer essentially the same value from the measured low-frequency dielectric constant. The Nb-atom spacing along the chains is $a_{\parallel} \approx 3.5$ Å, so that $L/a_{\parallel} \approx 6 \times 10^3$. According to our interpretation, this approximates the average impurity spacing, corresponding to a density $n_i \approx 175$ ppm or about 0.02%. The transverse phase correlation distance is then expected to be roughly $(6 \times 10^3)^{1/3} (80\ \text{Å}^2)^{1/2} \approx 160$ Å. This compares favorably with the estimate of ≈ 200 Å made by Fung and Steeds. The model we shall present here is thus capable of producing good agreement with existing experimental evidence on phase correlation in $NbSe_3$, based only on the measured value of the low-frequency dielectric constant.

Indirect evidence on the volume of a velocity-coherent region in $NbSe_3$ can also be obtained from the amplitude of the current oscillations, or narrow-band noise, which accompany CDW motion in a dc electric field. According to the above estimates, the volume of an individual region is roughly $2\ \mu{\rm m} \times (160\ \text{Å})^2 \approx 5 \times 10^{-4}\ \mu{\rm m}^3$. A typical small $NbSe_3$ crystal of the type used in our recent current oscillation experiments[30] has a total volume of order $1\ {\rm mm} \times 10\ \mu{\rm m} \times 1\ \mu{\rm m} \approx 10^4\ \mu{\rm m}^3$, and would thus contain $\sim 10^7$ velocity-coherent domains. The amplitude of

the externally observed current oscillations should thus be reduced by a factor of order $(10^7)^{-1/2}\approx 3\times 10^{-4}$, so that their absolute magnitude for a 1-mm-long sample with $E_T\approx 0.1$ V/cm would be $\sim 3\ \mu$V, in agreement with experiment.

A crucial feature of the present analysis is that the average phase $\bar{\phi}(r)$ will remain correlated over regions that are much larger than the volume n_i^{-1} per strong impurity. According to the above estimate, the total number of strong-pinning centers within a single phase-coherent domain is roughly

$$N_i\approx(\bar{L}/a_{\parallel})^{2/3}\approx 200[\bar{L}(\mu\text{m})]^{2/3}\ . \tag{2.20}$$

This result is initially very surprising. The common notion that the CDW phase is smoothly interpolated between strong-pinning sites has, we believe, led most people to conclude that the domain volume should be n_i^{-1}. When experiments showed this estimate to be at least 2 orders of magnitude too small, theoretical efforts became exclusively devoted to models of weak pinning. We are proposing here to revive the idea of strong pinning, together with CDW motion by phase slip, and will demonstrate in the following sections how this picture can be used to interpret a very broad range of experimental observations.

III. LOW-FREQUENCY POLARIZATION

The polarization of a CDW system in a dc electric field below threshold can be used to accurately infer the phase correlation length L for displacements along the chain direction. We have argued above that for strong pinning, L should be comparable to $\bar{L}$, the average spacing between impurities along a single chain. In this section, we shall develop a simple model for calculating the polarization in terms of this phase correlation length. Values of L inferred from dielectric measurements on intentionally doped o-TaS_3 crystals are then found to be in very good agreement with the average impurity spacing $\bar{L}$ calculated from the doping concentration. Furthermore, the prediction for the CDW angular displacement in a dc field just below threshold agrees precisely with a surprising result obtained in recent NMR experiments on $NbSe_3$.

To begin, we consider the polarization along a single chain within the context of a one-dimensional model. Considering only phase variations, the Hamiltonian for this system takes the form

$$H=\int dz\left[\tfrac{1}{2}K\left|\frac{\partial\phi}{\partial z}\right|^2-\frac{\rho_0}{Q}E\phi(z)+\sum_i V_i(z-z_i)\rho(z)\right]\ . \tag{3.1}$$

The first term here is the gradient energy for phase deformations along the chain axis. According to Eq. (2.1), the stiffness constant is given at low temperatures by[41]

$$K=2f_0\xi_{\parallel}^2A_0\approx\frac{\hbar v_F}{2\pi}\ . \tag{3.2}$$

The second term in Eq. (3.1) represents the coupling of the CDW to an applied electric field. Advancing the phase by 2π displaces the total CDW charge density ρ_0 through one wavelength, $\lambda_{\rm CDW}=2\pi/Q$, thereby lowering the potential energy by $\rho_0E\lambda_{\rm CDW}$ per unit volume. Here $Q=2k_F$ represents the wave vector that spans the one-dimensional Fermi surface. At temperatures well below T_p, $\rho_0\approx 2e/\lambda_{\rm CDW}$ so that

$$\frac{\rho_0}{Q}\approx\frac{e}{\pi}\ . \tag{3.3}$$

The final term in Eq. (3.1) characterizes the effects of pinning by impurities located at positions $\{z_i\}$ along the chain. We shall assume that $V_i(z-z_i)=V_i\delta(z-z_i)$, where V_i is taken to be strong enough to pin the CDW phase to its optimal value ϕ_0^i at each impurity site under all conditions. dc motion is then made possible only by phase slip.

In this one-dimensional model, the CDW polarizes freely between impurity sites according to

$$\frac{\delta H}{\delta\phi}=K\frac{d^2\phi}{dz^2}+\frac{\rho_0}{Q}E=0\ . \tag{3.4}$$

The solution for $\delta\phi(\pm L/2)=0$ is given by

$$\delta\phi(z)=\frac{eE}{\hbar v_F}[(L/2)^2-z^2]\ . \tag{3.5}$$

This result is sketched in Fig. 2. The average angular displacement of the CDW over a length L between two strong-pinning centers is calculated to be

$$\delta\bar{\phi}=\frac{1}{L}\int_{-L/2}^{L/2}dz\,\delta\phi(z)=\frac{eL^2E}{6\hbar v_F}\ . \tag{3.6}$$

This is two-thirds of the maximum displacement at $z=0$.

The dielectric constant can now be obtained from the average polarization along a single chain:

$$P=\frac{\rho_0}{A_0}\frac{\overline{\delta\phi}}{Q}=\frac{e^2L^2E}{6\pi\hbar v_FA_0}\ . \tag{3.7}$$

Equating this expression to ϵE yields the following result:

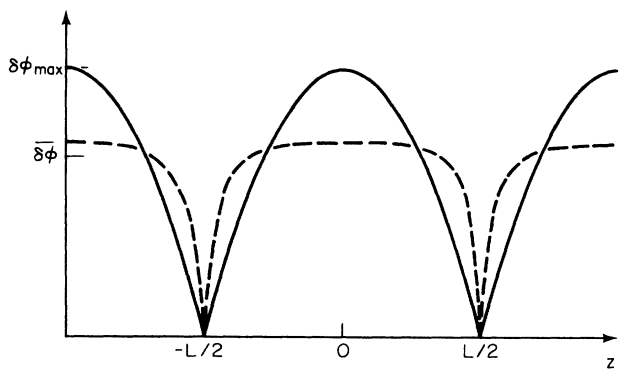

FIG. 2. Phase displacement in a dc electric field below threshold as a function of distance along the chain direction for a one-dimensional CDW pinned at $z=\pm L/2$, according to Eq. (3.5). Dashed curve indicates expected modification within a three-dimensional crystal.

$$\epsilon(\omega\rightarrow 0)=\frac{e^2L^2}{6\pi\hbar v_F A_0}=(1.45\times 10^7\epsilon_0)\frac{[L(\mu\text{m})]^2}{[v_F(10^7\text{ cm s}^{-1})][A_0(10^{-14}\text{ cm}^2)]}\ , \tag{3.8}$$

where $\epsilon_0=8.85\times 10^{-14}$ F/cm.

This expression for the low-frequency dielectric constant in terms of the phase correlation length L is essentially generic. It should be applicable to models of weak pinning as well, in which case L would represent the characteristic length scale discussed by Lee and Rice. The key feature here is that we identify this phase correlation length L with the average impurity spacing $\bar{L}$ along a single chain. In the preceding section, we argued for this result on the basis that most of the phase adjustment between the average $\bar{\phi}(r)$ and the pinned value ϕ_0^i at each impurity site will be made over a very small volume that is effectively confined to a single chain. If this is true, then individual impurities cannot strongly pin the phase on neighboring chains, and the phase correlation length should therefore be approximately given by the average impurity spacing.

Within the context of our polarization calculation, we expect that the angular displacement will be approximately equal to $\overline{\delta\phi}$ everywhere throughout the crystal. Inclusion of the transverse coupling between the chains should not greatly affect this average value. The detailed spatial dependence of $\delta\phi(z)$ along any individual chain will, however, be somewhat altered in the three-dimensional system from the form given in Eq. (3.5). The dashed curve in Fig. 2 indicates our qualitative expectation, with most of the difference between $\delta\phi(z)$ and $\overline{\delta\phi}$ resolved within the immediate vicinity of each impurity. The energy cost for this deformation will be somewhat higher than for the optimum one-dimensional distortion. The effect of the interchain coupling will thus act to reduce the effective value of L below the average spacing $\bar{L}$. If our arguments are correct, however, this reduction is expected to be relatively small.

The form for the dielectric constant given in Eq. (3.8) can be easily related to a more familiar result obtained from the simple damped oscillator model.[9,10] Lee, Rice, and Anderson[42] have shown that phase disturbances in an unpinned CDW system will propagate along the chain direction at a velocity

$$c_0=\left[\frac{m_b}{M_F}\right]^{1/2}v_F\ . \tag{3.9}$$

The average pinning frequency for standing waves confined to a mean distance L is therefore given by

$$\bar{\omega}_p=\frac{\pi c_0}{L}\ . \tag{3.10}$$

Inserting this relation into Eq. (3.8) then yields

$$\epsilon(\omega\rightarrow 0)=\frac{\pi^2}{12}\frac{n_c e^2}{M_F\bar{\omega}_p^2}=(6.7\times 10^7\epsilon_0)\frac{n_c(10^{21}\text{ cm}^{-3})}{(M_F/10^3 m_e)[\bar{\omega}_p/2\pi(\text{GHz})]^2}\ , \tag{3.11}$$

where $n_c=2k_F/\pi A_0$ represents the condensate electron density well below the Peierls transition. Except for the factor of $\pi^2/12$, this expression is seen to be identical to the corresponding result of the damped oscillator model.

Equation (3.8) allows an estimate for the phase correlation length L to be obtained from the measured value of $\epsilon(\omega\rightarrow 0)$. As an example, the dielectric constant is measured to be $\epsilon\approx 3\times 10^7\epsilon_0$ on the upper $NbSe_3$ CDW transition.[43] Assuming that two conducting chains within the 10.0×15.6 Å^2 unit cell participate gives $A_0\approx 78$ Å^2. The longitudinal bandwidth estimate $W_\parallel\approx 1.8$ eV from Table I predicts the Fermi velocity in Eq. (2.3) as $v_F\approx 3.2\times 10^7$ cm s^{-1}. Inserting these values into Eq. (3.8) gives $L\approx 2.3$ μm, in excellent agreement with the estimate $L\approx 2$ μm made by Fung and Steeds.[40]

Our estimate for the phase correlation length L can be used in Eq. (3.10) to infer the average pinning frequency. For this we require values of the inertial Fröhlich mass, which are now available from analyses of the roll-off in ac conductivity over the millimeter-wave region. The value obtained for $NbSe_3$ at 130 K and listed in Table I is $M_F/m_e\approx 300$. Combining this with the above estimates for L and v_F, Eqs. (2.4), (3.9), and (3.10) yield $\bar{\omega}_p/2\pi\approx 3.6$ GHz. This value is in excellent agreement with the results[34] $\omega_p/2\pi\approx 3$–6 GHz obtained by fitting the complete experimental ac response over the frequency range 1 MHz $<\omega/2\pi<$ 100 GHz to a damped oscillator model. The actual form of the ac conductivity as a function of frequency will be considered in detail in Sec. V.

To complete our discussion of the dielectric response in $NbSe_3$, we note that the expression given in Eq. (3.6) can also be used to interpret a rather surprising result obtained by Ross, Wang, and Slichter[44] in their recent NMR experiments. In terms of Eq. (3.8), the predicted angular displacement may be written in the form

$$\overline{\delta\phi}=\frac{\pi}{e}\epsilon(\omega\rightarrow 0)A_0E\ . \tag{3.12}$$

Using the experimental value $\epsilon\approx 3\times 10^7\epsilon_0$ and $A_0\approx 78$ Å^2, an electric field $E\approx 0.1$ V/cm close to the dc threshold for the upper $(NbSe_3)^I$ CDW should produce an average angular displacement $\overline{\delta\phi}\approx 2°$. This is precisely the result that Ross *et al.* obtained using pulsed NMR techniques with an applied dc field $E\approx 0.75E_T$. Such a small displacement near threshold is very anomalous from the viewpoint of a simple damped oscillator model, in which the angular displacement would be $\delta\phi\approx 50°$ at $E\approx 0.75E_T$. A great virtue of the present theory is its ability to quantitatively account for all of the important results obtained by Ross *et al.* in the course of their NMR studies of $NbSe_3$. We shall return to a more detailed consideration of these experiments in Sec. VII on

TABLE II. Comparison between experimental measurements and theoretical predictions for pure and intentionally doped o-TaS_3 crystals at $T=160$ K.

	Experiment				Theory		
	ϵ/ϵ_0[a]	E_T (V/cm)[a]	$\omega_p/2\pi$ (GHz)[b]	$\bar{L}$ (μm)	L (μm)	$\bar{\omega}_p/2\pi$ (GHz)	E_0 (V/cm)
Pure	3×10^7	0.5	5–8		1.3	3.9	0.75
0.1% Nb	6×10^6	3	35	0.33	0.57	8.7	2.3
0.2% Nb	5×10^5	25	120	0.16	0.17	30	11

[a] Reference 45.
[b] Reference 46.

the current oscillations.

In order to test our assertion that the phase correlation length L is related to the spacing $\bar{L}$ between impurities, we shall now analyze experimental data shown in Table II for Nb-doped o-TaS_3 crystals grown at UCLA. To our knowledge, this provides the only instance in which dielectric constant, dc threshold field, and millimeter-wave ac-conductivity measurements have all been published for intentionally doped crystals taken from the same growth batch. The dielectric and dc threshold data have been extracted from Wu *et al.*[45] and the millimeter-wave results from Reagor and Grüner.[46]

The parameter estimates we have used for o-TaS_3 are listed in Table I. The crystal structure is unknown, so we have first estimated $\bar{\omega}_p/2\pi$ using Eq. (3.11) and then calculated the phase correlation length L from Eq. (3.10). The results are listed in Table II, along with the experimental data. The experimental values for the pinning frequency are seen to be systematically larger than our estimates for $\bar{\omega}_p/2\pi$ by a factor of 2–4. This apparent discrepancy will be largely resolved in the course of our detailed discussion of the ac conductivity contained in Sec. V. Here we note the excellent agreement obtained between the calculated values of L and the average impurity spacing $\bar{L}$ given by the nominal Nb concentration. Without an assay, we cannot be certain that the nominal concentrations accurately reflect the actual impurity densities. Nevertheless, the close correspondence seen here between L and $\bar{L}$ is significant evidence in favor of our basic approach.

IV. DIELECTRIC RELAXATION

The polarization of the CDW was calculated in the preceding section in the limit of a static electric field. At finite frequencies, the dielectric response function is related to the small-signal ac conductivity according to

$$\epsilon(\omega)=\epsilon_0+\frac{\sigma(\omega)}{i\omega}\ . \tag{4.1}$$

In Fig. 3, we show our experimentally measured values of $\sigma(\omega)$ for a crystal of orthorhombic TaS_3 at 150 K. The dielectric response function $\epsilon(\omega)$ calculated according to Eq. (4.1) is shown in Fig. 4. The magnitude of $\mathrm{Re}\epsilon(\omega)$ is seen to approach its limiting static value $\epsilon(\omega\to0)\approx7\times10^7\epsilon_0$ at the lowest frequencies, but rolls off quickly above ~10 MHz. The position of this roll-off marks the dielectric relaxation frequency ω_0, which can be roughly estimated from the peak in $\mathrm{Im}\epsilon(\omega)$ near $\omega_0/2\pi\approx15$ MHz.

The solid curves in Figs. 3 and 4 represent the predictions of our strong-pinning theory, based upon the results that we derive for ac conductivity in Sec. V. The theoretical curves shown here were generated by convolving the ac-conductivity expression for a damped harmonic oscillator, given in Eq. (5.2), with the distribution in pinning frequencies obtained in Eq. (5.4). The only material parameters required are the average pinning frequency $\bar{\omega}_p/2\pi=3.9$ GHz, calculated in Table II for nominally pure o-TaS_3, and the damping parameter $1/2\pi\tau=120$ GHz inferred from the roll-off in experimental ac-conductivity data[46] at frequencies above ~10 GHz. The spectacular agreement seen in Figs. 3 and 4 is tempered only by a small discrepancy of ~2 between our measured value for $\epsilon(\omega\to0)$ and the result of Wu *et al.*[45] quoted in Table II, although the threshold fields and ac-conductivity data are closely similar for the two different crystals.

The physical nature of the dielectric relaxation frequency can be nicely illustrated within the context of our model. For this purpose, we return to the one-dimensional Hamiltonian given in Eq. (3.1). Assuming the system to be overdamped, the equation of motion,

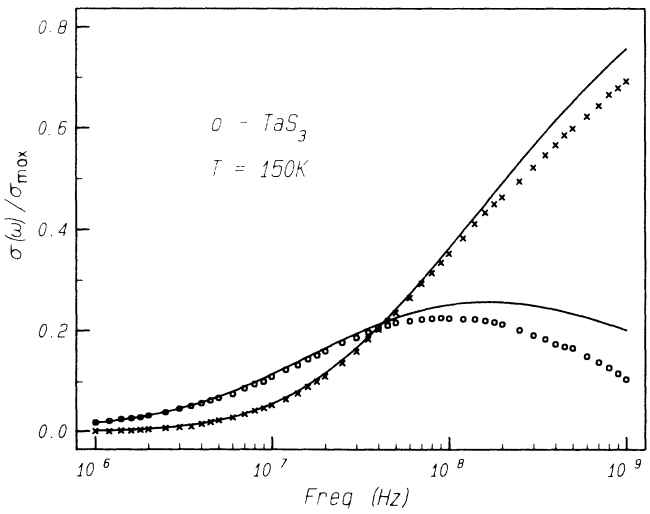

FIG. 3. Real (×) and imaginary (○) parts of the nonlinear ac conductivity as a function of frequency for a crystal of pure o-TaS_3 at $T=150$ K. Solid lines are predictions of the theory using $\bar{\omega}_p/2\pi=3.9$ GHz, $1/2\pi\tau=120$ GHz, and taking $\sigma_{\max}(150\ \mathrm{K})$ approximately equal to the room-temperature conductivity.

$\lambda\dot{\phi}=-\delta H/\delta\phi$, that determines the phase in regions between the strong impurities becomes

$$\lambda\frac{\partial\phi}{\partial t}=K\frac{\partial^2\phi}{\partial z^2}+\frac{\rho_0}{Q}E(t)\ . \tag{4.2}$$

The viscosity coefficient λ can be related to a CDW relaxation time τ according to

$$\lambda=M_F/\pi Q\tau\ . \tag{4.3}$$

With this definition, the limiting dc high-field CDW drift velocity is given by the standard expression, $Q^{-1}(\partial\phi/\partial t)\rightarrow eE\tau/M_F$.

Consider now the relaxation of a phase displacement within the average length L between two strong impurities. For zero electric field, a transient solution to Eq. (4.2) may be obtained in the form

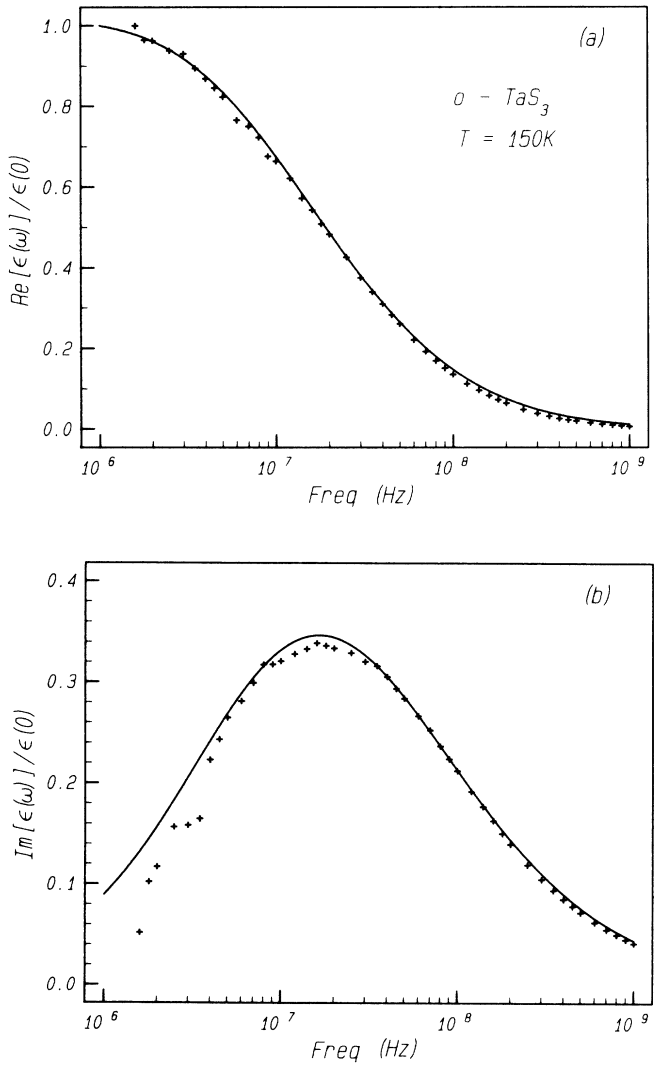

FIG. 4. (a) Real and (b) imaginary parts of the dielectric response as a function of frequency for a crystal of pure o-TaS_3 at $T=150$ K, calculated from the experimental results shown in Fig. 3 according to Eq. (4.1). Solid lines are again predictions of the theory using $\bar{\omega}_p/2\pi=3.9$ GHz and $1/2\pi\tau=120$ GHz.

$$\delta\phi(z,t)=\delta\phi_0 e^{-\omega_0 t}\sin(\pi z/L)\ . \tag{4.4}$$

The dielectric relaxation frequency is thereby estimated to be

$$\omega_0=\frac{\pi^2 K}{\lambda L^2}=\bar{\omega}_p^2\tau\ . \tag{4.5}$$

Here the average undamped pinning frequency is given by $\bar{\omega}_p=\pi c_0/L$, as in Eq. (3.10). This expression for the dielectric frequency ω_0 is thus seen to be identical to the "crossover frequency" for an overdamped oscillator with pinning frequency $\bar{\omega}_p$. Inserting the estimates quoted above for o-TaS_3 at $T=160$ K into Eq. (4.5) yields $\omega_0/2\pi\approx 125$ MHz. This value is close to the experimental crossover frequency defined by the maximum in $\mathrm{Im}\sigma(\omega)$ in Fig. 3. The actual dielectric relaxation frequency, however, is seen to be $\omega_0/2\pi\approx 15$ MHz from the maximum of $\mathrm{Im}\epsilon(\omega)$ in Fig. 4. The substantial difference between these two characteristic frequencies, which are identical for a single overdamped oscillator, results from the distribution in pinning frequencies given in Eq. (5.4) for the different CDW segements contained within the crystal.

The estimate for the dielectric relaxation frequency in Eq. (4.5) can be cast into an alternate form by using the relation

$$\lambda^{-1}=\frac{\pi^2 A_0\sigma_b}{e^2}\ , \tag{4.6}$$

where $\sigma_b=n_c e^2\tau/M_F$ represents the maximum high-field and high-frequency CDW conductivity. The resulting expression may then be written:

$$\omega_0=\frac{\pi^2}{12}\frac{\sigma_b}{\epsilon(\omega\rightarrow 0)}\ , \tag{4.7}$$

where we have utilized Eq. (3.8) for the static dielectric constant. In all common sliding CDW materials except $NbSe_3$, the Fermi surface is completely gapped below the Peierls transition. The concentration of thermally excited normal electrons will then decrease rapidly at low temperatures according to $n\sim\exp(-\Delta/k_B T)$. Eventually, the normal carrier concentration will become so small that the CDW charge fluctuations resulting from polarization and motion of the condensate cannot be screened by slight expansions and compressions in the normal electron density. When this occurs, the dissipation for low-frequency CDW motion will become dominated by that of the normal electrons, which must now flow over comparable distances in order to provide the required Coulomb screening. Under these conditions the normal conductivity $\sigma_N(T)$ effectively replaces σ_b in Eq. (4.7) and

$$\omega_0\approx\frac{\sigma_N(T)}{\epsilon(\omega\rightarrow 0)}\ . \tag{4.8}$$

Because $\sigma_N(T)$ is temperature activated, the dielectric relaxation frequency will decrease rapidly at low temperatures according to an Arrhenius behavior in those materials which undergo a complete metal-insulator transition.

A more detailed appreciation of this result may be obtained by relating the present picture of CDW polarization to our previous RC circuit model.[47] In Fig. 5, we have again sketched the form of Eq. (3.5) for CDW polarization within the context of the one-dimensional theory. Deformations of the CDW phase cause variations in the condensate charge density according to

$$\delta\rho_c(z)=\frac{e}{\pi}\frac{\partial\phi(z)}{\partial z} \tag{4.9}$$

per chain.

The charge $\tilde{Q}$ that is transferred from left to right across $z=0$ in Fig. 5 may then be calculated as

$$\tilde{Q}=\frac{e^2L^2E}{4\pi\hbar v_F} . \tag{4.10}$$

If we now associate the voltage $V=EL$ with the potential drop across this length, the charge may be written as $\tilde{Q}=\frac{1}{2}C_pV$ where $C_p=\epsilon(\omega\to 0)A_0/L$ defines the polarization capacitance associated with this region. The average length over which charge must move when $\tilde{Q}$ changes is found to be $L_s=\frac{2}{3}L$ within this model. At low temperatures in CDW materials with a completely gapped Fermi surface, the normal electrons that are "frozen" onto the CDW charge variations must also move over a comparable distance. Their dissipation thus leads to an effective CDW resistance $R_{\rm eff}\approx L_s/\sigma_N(T)A_0$ for the region in Fig. 5 that lies in series with the polarization capacitance C_p. The characteristic relaxation frequency is then given by the inverse RC time constant, $\omega_0=1/R_{\rm eff}C_p$, which reproduces the result quoted in Eq. (4.8) multiplied by $L/L_s\sim 1$:

$$\frac{\omega_0}{2\pi}\approx(1.8\times10^{12}\ \mathrm{s}^{-1})\frac{\sigma_N(\Omega^{-1}\,\mathrm{cm}^{-1})}{\epsilon(\omega\to0)/\epsilon_0}\frac{L}{L_s} . \tag{4.11}$$

Cava and co-workers[48–50] have recently performed a series of important experiments on the dielectric response of $(TaSe_4)_2I$, $K_{0.3}MoO_3$, and o-TaS_3 in the frequency range 5 Hz to 13 MHz. In each of these materials, they find that the dielectric relaxation frequency decreases with an Arrhenius behavior at low temperatures, and

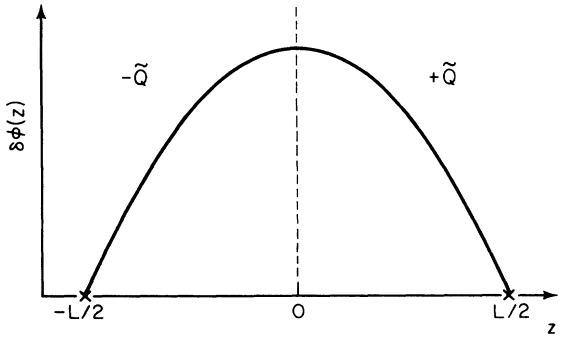

FIG. 5. Phase displacement in a dc electric field below threshold as a function of distance along the chain direction for a one-dimensional CDW pinned at $z=\pm L/2$, according to Eq. (3.5). A total charge $\tilde{Q}$ is transferred across $z=0$ by the CDW polarization.

these results have led us directly to the analysis summarized above. For $(TaSe_4)_2I$, the data of Cava *et al.*[48] covering the temperature range $90<T<180$ K may be accurately fitted by

$$\frac{\omega_0^{\rm expt}}{2\pi}=(1.0\times10^{10}\ \mathrm{s}^{-1})e^{-(1436\,\mathrm{K})/T} . \tag{4.12}$$

Over the same temperature range, their measured normal resistivity gives

$$\sigma_N(T)=(3.7\times10^3\ \Omega^{-1}\,\mathrm{cm}^{-1})e^{-(1434\,\mathrm{K})/T} . \tag{4.13}$$

Their experimental value for the low-frequency dielectric constant is $\epsilon(\omega\to0)\approx1\times10^6\epsilon_0$, roughly independent of temperature, so that the prediction of Eq. (4.11) becomes

$$\frac{\omega_0^{\rm theor}}{2\pi}\approx(0.7\times10^{10}\ \mathrm{s}^{-1})e^{-(1434\,\mathrm{K})/T}\frac{L}{L_s} , \tag{4.14}$$

in precise numerical agreement with experiment for $L_s\approx L$.

In $K_{0.3}MoO_3$, the data of Cava *et al.*[49] for $60<T<100$ K yield[51]

$$\begin{aligned}\frac{\epsilon(\omega\to0)}{\epsilon_0}&=(1.6\times10^6)e^{+(334\,\mathrm{K})/T} ,\\ \frac{\omega_0}{2\pi}&=(3.2\times10^9\ \mathrm{s}^{-1})e^{-(829\,\mathrm{K})/T} .\end{aligned} \tag{4.15}$$

Inserting these values into Eq. (4.11), we infer a normal conductivity:

$$\sigma_N^{\rm theor}(T)\approx(3.0\times10^3\ \Omega^{-1}\,\mathrm{cm}^{-1})e^{-(495\,\mathrm{K})/T}\frac{L_s}{L} . \tag{4.16}$$

Although Cava *et al.* did not published complete resistivity data for this particular sample, their data published in a subsequent paper[52] for pure $K_{0.3}MoO_3$ over the same temperature range give

$$\sigma_N^{\rm expt}(T)=(2.0\times10^3\ \Omega^{-1}\,\mathrm{cm}^{-1})e^{-(498\,\mathrm{K})/T} , \tag{4.17}$$

again in precise numerical agreement for $L_s\approx L$ with the prediction of our simple model. This last paper contains dielectric measurements on $K_{0.3}MoO_3$ crystals intentionally doped with Rb and W, and many of the features observed in these experiments can be understood on the basis of the simple functional relation given in Eq. (4.8).

According to our model, an Arrhenius temperature dependence of the dielectric relaxation frequency should be observed at low temperatures in all CDW materials which undergo a complete metal-insulator transition. At sufficiently high temperatures, on the other hand, we expect that ω_0 will be given by Eq. (4.7), and should therefore be approximately temperature independent. The boundary between these two regimes can be estimated by considering the density of normal carriers that are available to screen the CDW charge fluctuations. For a one-dimensional semiconductor with conduction-band energies

$$E_c(k)=\Delta+\frac{\hbar^2k^2}{2m^*} , \tag{4.18}$$

the thermally excited carrier density is given by

$$n(T)=2\left[\frac{m^*k_BT}{2\pi\hbar^2}\right]^{1/2}e^{-\Delta/k_BT}$$
$$=(2.68\times10^5\ \mathrm{cm}^{-1})\left[\frac{m^*}{m_e}\right]^{1/2}[T(\mathrm{K})]^{1/2}e^{-\Delta/k_BT}\ . \tag{4.19}$$

When a Peierls gap opens in the tight-binding band of Eq. (2.2), the quasiparticle spectrum in the neighborhood of the Fermi surface will be approximately given by $\varepsilon(k)=\pm[\Delta^2+(\hbar v_F k)^2]^{1/2}$ for $\Delta\ll W_\parallel$. Expanding this relation, we can identify the appropriate effective mass in Eq. (4.18) as

$$m^*=\Delta/v_F^2\approx(17.6m_e)\frac{\Delta(\mathrm{eV})}{[v_F(10^7\ \mathrm{cm\,s}^{-1})]^2}\ . \tag{4.20}$$

The number of normal electrons that are required in order to screen the CDW charge fluctuations corresponds to approximately one per phase correlation length L on each chain. When the average normal carrier density $n(T)$ falls below this value, those normal electrons which are screening the CDW charge fluctuations become effectively frozen onto the CDW phase gradients. For the CDW to polarize, these normal electrons must move over a comparable distance, and this leads to the Arrhenius behavior that we have characterized above. When $n(T)\gg1/L$ at higher temperatures, the dissipation associated with the normal screening is negligible. The temperature T_a at which the Arrhenius behavior sets in can therefore be estimated by the criterion $n(T_a)\approx1/L$:

$$[T_a(\mathrm{K})]^{1/2}\exp[-\Delta(T_a)/k_BT_a]$$
$$\approx(3.7\times10^{-2})\left[\frac{m^*}{m_e}\right]^{-1/2}\frac{1}{L(\mu\mathrm{m})}\ . \tag{4.21}$$

In Fig. 6 we show our experimental data for the dielectric relaxation frequency of the same orthorhombic TaS_3 crystal characterized in Figs. 3 and 4, this time as a function of temperature. Using the estimates $\Delta\approx0.06$ eV and $v_F\approx5\times10^7$ cm s^{-1} obtained from Table I in Eq. (4.20) gives $m^*/m_e\approx4.2\times10^{-2}$. Inserting this result into Eq. (4.21) along with the value $L\approx1.3$ μm estimated previously then yields $T_a\approx155$ K. In Fig. 6, the dielectric relaxation frequency is seen to be roughly temperature independent below 200 K until it breaks sharply into an Arrhenius behavior near $T_a\approx(1000\ \mathrm{K})/6.7\approx150$ K, in precise agreement with our estimate. All essential aspects of the dielectric relaxation behavior seen in sliding CDW materials thus appear to be accurately described by the present model.

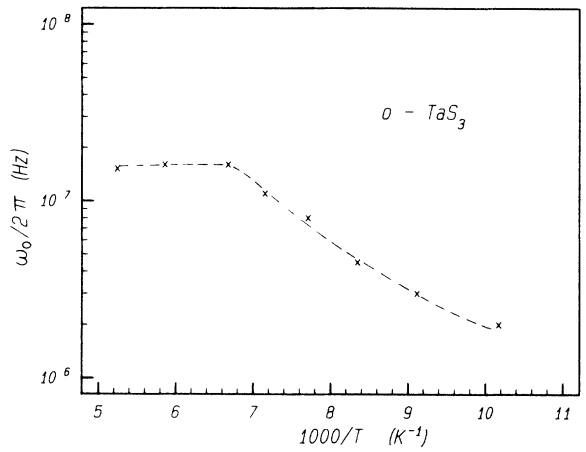

FIG. 6. Dielectric relaxation frequency as a function of temperature for pure o-TaS_3, obtained from the experimentally observed maximum in Im$\epsilon(\omega)$. Dashed line is a guide to the eye.

V. ac CONDUCTIVITY

The ac conductivity seen in sliding CDW systems has often been interpreted in terms of a simple damped oscillator. Displacements of the CDW along the chain axis are given by $\delta x=\delta\phi/Q$, so that the phenomenological equation of motion for CDW electrons is taken to be

$$\frac{M_F}{Q}\left[\frac{d^2\phi}{dt^2}+\frac{1}{\tau}\frac{d\phi}{dt}+\omega_p^2\sin\phi\right]=eE(t)\ . \tag{5.1}$$

Here it is assumed that the periodic pinning potential is sinusoidal, with an undamped natural frequency ω_p. For small fields, this model predicts an ac conductivity

$$\sigma(\omega)=\sigma_b\frac{i\omega/\tau}{(\omega_p^2-\omega^2)+i\omega/\tau}\ , \tag{5.2}$$

where $\sigma_b=n_ce^2\tau/M_F$ again represents the maximum CDW conductance.

ac-conductivity data for orthorhombic TaS_3 at $T=160$ K, covering the entire frequency range from 10 MHz to 100 GHz, are reproduced from Reagor and Grüner[46] in Fig. 7. The dashed curves represent their fit to the single-oscillator expression of Eq. (5.2) using $\omega_p/2\pi=5$ GHz and $1/2\pi\tau=120$ GHz. The roll-off at frequencies beyond ~10 GHz is due to the inertia term in Eq. (5.1), and their fit to the data in this millimeter-wave region is very good. On the other hand, the rise in ac conductivity at frequencies below ~1 GHz is clearly much too broad to be described by a single oscillator. In a subsequent publication,[35] the data in Fig. 7 were fitted reasonably well by assuming a distribution of pinning frequencies with relative weight $P(\omega_p)=1$ for $\omega_p/2\pi\leq5$ GHz and $P(\omega_p)=0$ at higher frequencies.

The discussion of the preceding sections has focused on the phase correlation length L along the chain axis, and the associated average pinning frequency $\bar{\omega}_p=\pi c_0/L$. We have argued that for strong pinning and small impurity concentrations, this correlation length should approximate the average spacing $\bar{L}$ between consecutive impurities along any individual chain. There will, of course, be a distribution in the lengths l between particular impurities given by

$$P(l)=\frac{1}{L}e^{-l/L}\ . \tag{5.3}$$

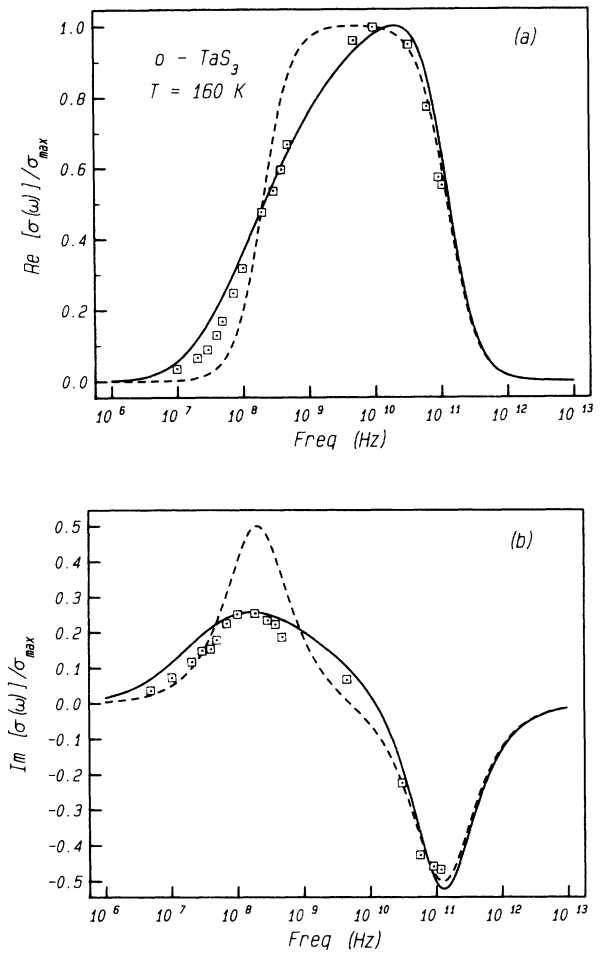

FIG. 7. (a) Real and (b) imaginary parts of the ac conductivity as a function of frequency for pure o-TaS_3 at $T=160$ K. Solid curves are predictions of the theory using $\bar{\omega}_p/2\pi=3.9$ GHz and $1/2\pi\tau=120$ GHz. Dashed curves represent a single damped oscillator fit with $\omega_p/2\pi=5$ GHz. Experimental data points are reproduced from Sridhar *et al.* (Ref. 35).

If each segement can be considered to respond independently, the corresponding distribution in pinning frequencies $\omega_p=\pi c_0/l$ becomes

$$P(\omega_p)=\frac{\bar{\omega}_p}{\omega_p^2}e^{-\bar{\omega}_p/\omega_p}\ . \tag{5.4}$$

We have argued in Secs. II and III that an individual segment cannot polarize independently at low frequencies, so that the static dielectric constant reflects only the average correlation length L. An inspection of Eqs. (5.1) and (5.2), however, reveals that for an overdamped system, the maximum ac conductivity is approached only when the viscosity term exceeds the restoring force due to pinning. This is seen to occur for $\omega>\omega_p^2\tau$, when the applied frequency exceeds the "crossover frequency" of the overdamped oscillator. In this region, pinning ceases to play a significant role in determining the ac conductivity, and the response is essentially that of an ideal unpinned CDW subject to damping, and eventually to inertia. If we now consider the behavior of an individual segment of length l located between two impurities, it becomes clear that this region cannot contribute its maximum to the ac response until $\omega>(\pi c_0/l)^2\tau$, since at lower frequencies it must still feel significant effects of the impurity pinning. On this basis, we expect that the distribution of pinning frequencies given in Eq. (5.4) should, in fact, provide a reasonably accurate description for the shape of the ac conductivity as a function of frequency.

The solid curves in Fig. 7 are obtained by convolving the distribution of pinning frequencies given in Eq. (5.4) with the damped oscillator response of Eq. (5.2). Here we have used the value $\bar{\omega}_p/2\pi=3.9$ GHz obtained in Table II for nominally pure o-TaS_3, together with the experimental damping parameter $1/2\pi\tau=120$ GHz. The fit to the data is seen to be remarkably accurate over this entire frequency range. The nominal crossover frequency in this case is given by $\bar{\omega}_p^2\tau/2\pi\approx 125$ MHz, and the peak in $\mathrm{Im}\sigma(\omega)$ is seen in Fig. 7(b) to occur at a slightly higher frequency near ~ 150 MHz. The theoretical predictions shown in Fig. 7 are the same ones that were used to fit the ac-conductivity and dielectric response data for a comparable o-TaS_3 crystal at $T=150$ K in Figs. 3 and 4.

Experimental ac-conductivity data are also available on $NbSe_3$ out to the millimeter-wave region.[34] The results for both CDW's are very similar to the data shown for o-TaS_3 in Fig. 7. The estimate $\bar{\omega}_p/2\pi\approx 3.6$ GHz that we have obtained in Sec. III for the $(NbSe_3)^I$ CDW can be used in conjunction with the damping parameter $1/2\pi\tau=105$ GHz inferred from the millimeter-wave roll-off to produce predictions that are as accurate as those obtained above for o-TaS_3.

The ac-conductivity data[36] on $(TaSe_4)_2I$ displays a very different behavior. Figure 8 illustrates the results of measurements at 150 K by Reagor *et al.*[53] covering a large frequency range 1 kHz $\leq\omega/2\pi\leq$ 100 GHz. The millimeter-wave data indicate a single-oscillator reso-

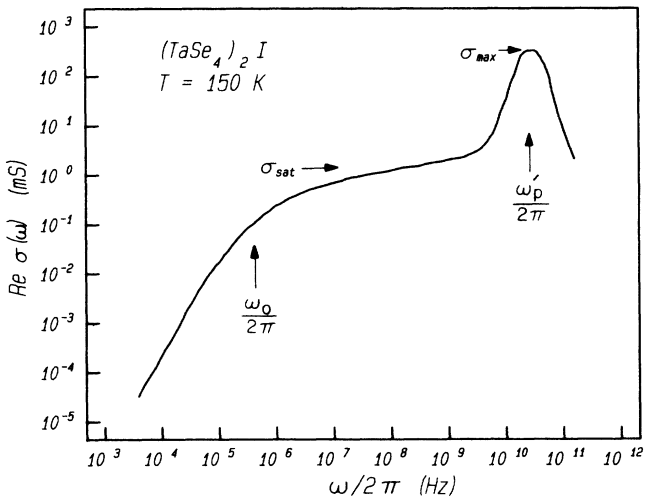

FIG. 8. ac-conductivity data for a crystal of $(TaSe_4)_2I$ at $T=150$ K, covering the extensive frequency range 1 kHz $<\omega/2\pi<$ 100 GHz. The millimeter wave resonance frequency $\omega_p'/2\pi\approx 34$ GHz and the dielectric relaxation frequency $\omega_0/2\pi\approx 1$ MHz are indicated, along with the maximum ac conductivity σ_{max} and the nearly constant value σ_{sat} for $\omega_0\ll\omega\ll\omega_p'$. Reproduced from Reagor *et al.* (Ref. 53).

nance centered at $\omega_p'/2\pi \approx 34$ GHz, with a damping parameter given by $1/2\pi\tau \approx 21$ GHz. Below ~ 1 GHz, the ac conductivity is seen to be nearly independent of frequency, with $\sigma_{\rm sat} \sim 10^{-3}\ \sigma_{\rm max}$ all the way down to the dielectric relaxation near $\omega_0/2\pi \approx 1$ MHz. Below this dielectric relaxation frequency, $\mathrm{Re}\sigma(\omega) \sim \omega^2$ and $\mathrm{Re}\epsilon(\omega)$ approaches its static value. The magnitude of $\sigma_{\rm sat}$ and $\omega_0/2\pi$ are both observed to decrease rapidly with temperature according to an Arrhenius behavior, displaying an activation energy $\Delta/k_B \approx 1400$ K determined by the Peierls gap.

The dielectric relaxation frequency $\omega_0/2\pi \approx 1$ MHz seen in Fig. 8 for $(TaSe_4)_2I$ at 150 K is consistent with the low-frequency measurements of Cava *et al.*[48] that we have characterized in Eq. (4.12) of the preceding section. There we showed that these experimental values for the dielectric frequency could be predicted from Eq. (4.8), based on the notion that normal carrier screening effectively dominates the CDW dissipation at low temperatures. According to this model, we would also predict that $\sigma_{\rm sat} \sim \sigma_N(T)$. All modes which involve a spatially dependent polarization of the CDW should be subject to greatly enhanced dissipation associated with the Coulomb screening process at low temperatures. In this regard, it is interesting to note that the high-field dc conductance measured by Fleming *et al.*[54] also follows the normal conductivity $\sigma_N(T)$ in $(TaSe_4)_2I$, as well as in TaS_3 and $K_{0.3}MoO_3$ at low temperatures. This behavior directly reflects the polarizations of the CDW that accompany dc motion by the phase-slip process, as described in the following section.

The single underdamped mode at $\omega_p'/2\pi \approx 34$ GHz in Fig. 8 is *not* subject to the huge increase in damping associated with normal electron screening. Millimeter-wave data taken as a function of decreasing temperature[36] show a slight *increase* of the maximum conductivity near $\omega_p'/2\pi \approx 34$ GHz, with $\sigma_{\rm max}$ close to the room-temperature value $\sigma_{\rm RT} \approx 350\ \Omega^{-1}\,\mathrm{cm}^{-1}$ for all $T \gtrsim 30$ K.

The average pinning frequency in $(TaSe_4)_2I$ can be inferred by inserting the measured[48] static dielectric constant $\epsilon(\omega \to 0) \approx 1 \times 10^6 \epsilon_0$ into Eq. (3.11), along with the estimates for n and M_F/m_e contained in Table I. The result of this calculation yields $\bar{\omega}_p/2\pi \approx 4.6$ GHz, much lower by a factor of ~ 7–8 than the resonance seen at $\omega_p'/2\pi \approx 34$ GHz in Fig. 8. The average pinning frequency $\bar{\omega}_p/2\pi = c_0/2L$, as we have defined it, refers to large-scale polarizations of the average phase $\bar{\phi}(r)$. At low temperatures, restricted normal electron screening drives the effective crossover frequency for these modes down rapidly according to $\omega_0 \approx \sigma_N(T)/\epsilon(\omega \to 0)$, producing a highly overdamped contribution to the ac conductivity with a greatly reduced $\sigma_{\rm sat} \sim \sigma_N(T)$. The unscreened mode seen at $\omega_p'/2\pi \approx 34$ GHz is, we believe, not associated with these large-scale polarizations of the average phase, but with oscillation of the smaller phase ripples that occur on a volume scale n_i^{-1} surrounding each individual impurity. According to Eq. (2.18), the amplitude of these interpolations of the average phase $\bar{\phi}(r)$ toward the pinned values ϕ_0^i at each strong pinning site should be relatively small for dilute impurity concentrations $L \gtrsim 0.3$ μm or $n_i \lesssim 1000$ ppm. When the large-volume $\bar{\phi}(r)$ modes are effectively frozen out, however, coherent oscillations of the phase ripples on the n_i^{-1} scale should produce a contribution to the ac conductivity that is much more easily screened. A rough numerical estimate of the associated resonance frequency can be obtained in terms of the approximate length scale $L_{\rm min}$ given by Eq. (B2) for the extent of these phase modulations along the chain direction:

$$\frac{\omega_p'}{2\pi} \approx \frac{c_0}{4L_{\rm min}} . \tag{5.5}$$

For $(TaSe_4)_2I$, this relation yields $\omega_p'/2\pi \approx (30\ \mathrm{GHz})/[\bar{L}(\mu\mathrm{m})]^{1/3}$, in excellent agreement with experiment for the values of $L \approx 0.5$ μm inferred from $\epsilon(\omega \to 0)$ for nominally pure material. Doping studies should easily distinguish between this low-temperature millimeter-wave resonance, $\omega_p' \sim n_i^{1/3}$, and the fully screened average pinning frequency $\bar{\omega}_p \sim n_i$ seen in $NbSe_3$ and in o-TaS_3 for $T \gtrsim 140$ K.

In all common sliding CDW materials except $NbSe_3$, the Fermi surface is completely gapped below the Peierls transition. At sufficiently low temperatures, therefore, each of these other materials should also display the same general features illustrated in Fig. 8 for $(TaSe_4)_2I$. The low-frequency dielectric response measured[49] in $K_{0.3}MoO_3$ for $60 < T < 100$ K indeed shows the characteristic Arrhenius dependence, as discussed in conjunction with Eqs. (4.15)–(4.17). Far-infrared reflectance measurements[55] on $K_{0.3}MoO_3$ also clearly establish a conductivity resonance near ≈ 84 GHz at liquid-He temperatures, which we tentatively identify with $\omega_p'/2\pi$. A simple theoretical interpretation is precluded, however, by an apparent commensurate transition[56] that occurs in $K_{0.3}MoO_3$ near 100 K. In o-TaS_3, the dielectric response again displays an Arrhenius-type behavior for $T < 150$ K, as shown in Fig. 6. But here also, both electron-diffraction studies[57] and dc-conductance data[54] indicate some type of commensurate transition setting in about 140 K, with perhaps a second transition to complete three-dimensional commensurability near 80 K. The large apparent increase in the pinning frequency of pure o-TaS_3 seen in the millimeter-wave data[35] for $T < 150$ K is, nevertheless, consistent with the freeze-out of the $\bar{\omega}_p/2\pi \approx 3.9$ GHz modes, leaving a single resonance in the general neighborhood of $\omega_p'/2\pi \sim 50$ GHz. This freeze-out occurs at higher temperatures in $(TaSe_4)_2I$ due to its much larger Peierls gap.[58]

VI. dc MOTION

In Sec. II, we estimated the pinning energy associated with an individual strong impurity to be

$$E_{\rm pin}(\bar{\phi} - \phi_0) \approx \frac{\Delta}{4\pi^2}(\bar{\phi} - \phi_0)^2 . \tag{6.1}$$

This result is sketched in Fig. 9, together with the corresponding curves for ϕ_0 displaced by integral multiples of 2π. When the average phase $\bar{\phi}$ surrounding the impurity

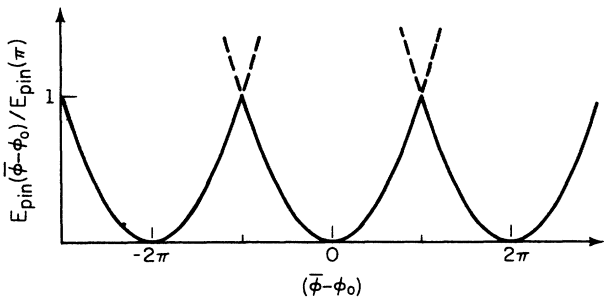

FIG. 9. Pinning energy associated with a single impurity as a function of displacement in the average CDW phase $\bar{\phi}$ relative to the pinned value ϕ_0 at the strong impurity site, according to Eq. (6.1).

increases beyond the pinned value ϕ_0, the elastic energy rises quadratically until the relative phase difference reaches π. At this point, a phase-slip process can transfer the system to a lower-energy configuration in which ϕ_0 is suddenly increased by 2π. We shall assume that this phase-slip process occurs instantaneously on experimental time scales, so that the effective potential due to a single impurity approximates the solid curve given by the intersecting parabolas in Fig. 9.

The basic aspects of phase slip are most easily illustrated by returning to the one-dimensional model of Sec. III. There the phase displacement of the CDW between two strong-pinning centers in a dc electric field was determined by Eq. (3.5) and sketched in Fig. 2. This model produces an abrupt discontinuity in the phase gradient at each impurity site:

$$\left.\frac{d\phi}{dx}\right|_{x=L/2\pm\varepsilon} = \pm\frac{eLE}{\hbar v_F} . \tag{6.2}$$

This discontinuity is an artifact of our phase-only approximation for the Hamiltonian in Eq. (3.1). We should really have written down the Ginzburg-Landau equation that comes from minimizing the total free-energy expression of Eq. (2.1), in which $\psi(x) = |\psi(x)| e^{i\phi(x)}$ is allowed to vary in amplitude as well as in phase. In one dimension and for $t=1$, setting $\delta F/\delta\psi^*(z)=0$ yields

$$-\psi+\psi|\psi|^2-\xi_z^2\frac{\partial^2\psi}{\partial z^2}=0 . \tag{6.3}$$

The inclusion of amplitude variations will affect the solution only within a very small region of order ξ_z about each strong-pinning site. For small electric fields, the average magnitude of the gradient term within these regions is given by

$$\xi_z^2\left|\frac{\partial^2\psi}{\partial z^2}\right| \approx \xi_z^2|\psi|\left[\frac{d\phi/dz\,|_{z=L/2+\varepsilon}-d\phi/dz\,|_{z=L/2-\varepsilon}}{\xi_z}\right] \approx \frac{2eLE}{\pi\Delta}|\psi| . \tag{6.4}$$

When this term reaches a value of order $\sim\frac{1}{2}|\psi|$, the state having $\psi=0$ within such a region will represent a lower-energy configuration and the order parameter will therefore collapse. The critical electric field for phase slip at $T=0$ is then roughly estimated as

$$E_0(0)\sim\frac{\pi}{4}\frac{\Delta}{eL} . \tag{6.5}$$

Returning now to our three-dimensional result for the effective impurity pinning potential in Eq. (6.1), we can make a more careful estimate of the electric field needed to induce dc motion by phase slip. Approximately equating the energy for displacing the phase by π at each pinning site to the potential gained by moving the CDW forward by $\lambda_{CDW}/2$ in the presence of the electric field yields

$$\gamma n_i E_{pin}(\pi)=n_c e E_0(0)\lambda_{CDW}/2 , \tag{6.6}$$

where the value of γ will be estimated below. Using $n_i=(A_0\bar{L})^{-1}$ and $n_c=2/\lambda_{CDW}A_0$, this result becomes

$$E_0(0)=\gamma\frac{\Delta}{4eL}=(2500\text{ V/cm})\gamma\frac{\Delta(\text{eV})}{L(\mu\text{m})} . \tag{6.7}$$

For $\gamma=1$, this value is seen to be smaller than the one-dimensional estimate of Eq. (6.5) by a factor of π.

The result given in Eq. (6.7) for $\gamma=1$ is still much too large. According to the analysis presented in Sec. II, the average phase $\bar{\phi}(r)$ will be only partially interpolated toward the pinned value ϕ_0^i in the neighborhood of each impurity when the system is in equilibrium. Substantial phase displacements are thus already built in at most impurity sites, and the value of γ should therefore be much less than unity. If the interpolation of $\bar{\phi}(r)$ toward the pinned value ϕ_0^i at each site is very small, then the electric field needs only to overcome fluctuations in the pinning energy within a phase-coherent volume. Under these conditions, $\gamma\approx 1/(N_i)^{1/2}$ where N_i represents the total number of impurities contained within this region. From Eq. (2.18), we estimate that the interpolation energy remains relatively large, so that $E_{elast}>3E_{pin}$, for an average impurity spacing of at least $L\gtrsim 0.3\ \mu$m. In this regime, the value for N_i given in Eq. (2.20) may be used to give

$$\gamma\approx 0.07[L(\mu\text{m})]^{-1/3} . \tag{6.8}$$

It is clear that this rough estimate may represent too large a reduction in the critical electric field, since some small interpolation of the average phase $\bar{\phi}(r)$ still takes place in the neighborhood of each impurity site. We shall, nevertheless, make use of it in analyzing the experimental data for relatively dilute impurity concentrations. Our estimate for the average depinning field thus becomes

$$E_0(0) \approx (175\ \text{V/cm}) \frac{\Delta(\text{eV})}{[L(\mu\text{m})]^{4/3}} . \quad (6.9)$$

It should be kept in mind that the resulting numerical estimates are likely to be somewhat too small, especially when $L < 0.3\ \mu$m or $n_i > 1000$ ppm.

Finite temperatures will substantially reduce the magnitude of the electric field needed in order to depin the CDW. This is apparent from Eq. (6.1), since the pinning energy at each impurity site is seen to be comparable to $k_B T$ at typical experimental temperatures. Independent local fluctuations of the CDW phase configuration will occur in the immediate neighborhood of every impurity, each mode approximately confined to the tiny volume containing the localized phase gradients at the various pinning sites as discussed in Sec. II. The effect of these thermal fluctuations on the pinning energy can be included very simply by modifying an argument originally applied to CDW systems by Maki.[59] This calculation is outlined in Appendix C. The temperature dependence of the depinning field is found to be of the form

$$E_0(T) = E_0(0) e^{-T/T_0} , \quad (6.10)$$

where the temperature scale within the present model is approximately

$$T_0 \approx \frac{4E_{\text{pin}}(\pi)}{\pi^2 k_B} \approx (1160\ \text{K}) \Delta(\text{eV}) . \quad (6.11)$$

This characteristic behavior of the threshold field with temperature is nicely illustrated in the data collected by Monceau[33] and reproduced in Fig. 10. The functional form predicted by Eq. (6.10) is seen to be followed in all of the materials represented here. The rapid divergence in E_T seen near each Peierls transition temperature results from the fact that the condensate electron density $n_c(T)$ vanishes more quickly than the energy gap $\Delta(T)$ as

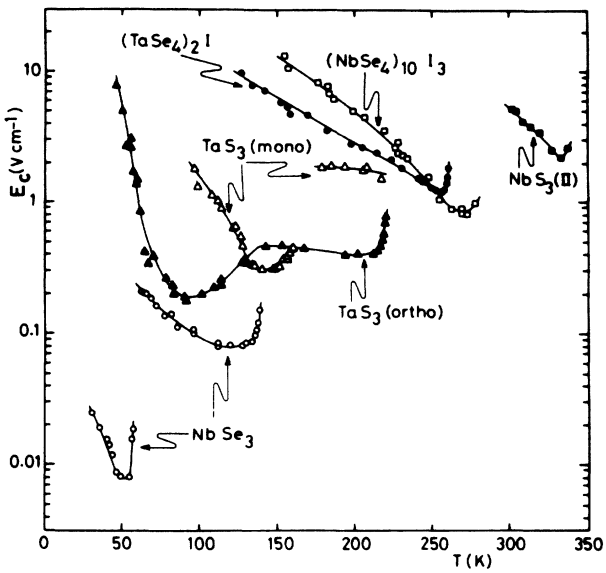

FIG. 10. Threshold field data as functions of temperature for representative crystals of several sliding CDW compounds. Reproduced from Monceau (Ref. 33).

$T \to T_p$, reducing the force of the electric field relative to the pinning. In mean-field theory, $n_c(T)$ is proportional to $\Delta^2(T)$ with $\Delta(T) \sim (T_p - T)^{1/2}$. The additional factor multiplying Eq. (6.10) would then be given by

$$\frac{\Delta(T)}{\Delta(0)} \frac{n_c(0)}{n_c(T)} \to \frac{1}{(1 - T/T_p)^{1/2}} \quad \text{as } T \to T_p . \quad (6.12)$$

The divergencies seen in the threshold fields near T_p in Fig. 10 appear much sharper than this mean-field prediction, for reasons which are quite understandable. One-dimensional fluctuations cause the expectation value of the average gap $\langle \Delta \rangle$ and the condensate density n_c to go to zero at $T_p \approx 0.3 T_p^{\text{MF}}$, far below the mean-field transition temperatures for these materials. The value of $\langle \Delta^2 \rangle$ does not go to zero at T_p, however, and fluctuation effects due to this pseudogap are observable well above T_p in most cases. In regions where the CDW phase is pinned down by a strong impurity, the magnitude of the gap should therefore tend to remain larger than the bulk value of $\langle \Delta \rangle$ as the temperature approaches T_p. The result presumably leads to the very sharp divergences seen in the threshold fields in Fig. 10 close to T_p.

Table III shows a comparison between the values of T_0 inferred from the experimental data in Fig. 10 and those calculated using Eq. (6.11). An experimental value is not listed for orthorhombic TaS_3 because of the unusual behavior apparent in Fig. 10, thought to be associated with the onset of a commensurate transition near $T = 140$ K. The correlation between the experimental and calculated estimates of T_0 appears to be reasonable, except that the theoretical predictions are apparently too large by a factor of 2–3 in the larger-gap materials. This problem actually arises because the measured threshold field E_T does not usually provide a reliable estimate for the average depinning field E_0, except in $NbSe_3$ where the abundance of normal carriers ensures very uniform electric fields and CDW drift velocities throughout the entire crystal volume. In $(TaSe_4)_2I$, for example, threshold field data published by Cava *et al.*[48] indicate that E_T is nearly temperature independent for $90 < T < 180$ K, while in Fig. 10 it is shown to change by a factor of ~ 4 over a comparable region. These discrepancies, as we shall demonstrate below, can be largely resolved by fitting the complete dc

TABLE III. Comparison between the experimental temperature dependences $\exp(-T/T_0)$ seen in the data of Fig. 10 and the theoretical predictions of Eq. (6.11). The values labeled with an asterisk for Δ in $NbSe_3$ are estimated by scaling from the o-TaS_3 gap according to the ratio of the transition temperatures.

	Δ (eV)	T_0^{theor} (K)	T_0^{expt} (K)
$(NbSe_3)^{II}$	1.6×10^{-2} *	19	~20
$(NbSe_3)^{I}$	3.9×10^{-2} *	45	~40
TaS_3 (ortho)	6.0×10^{-2}	70	
TaS_3 (mono)	8.2×10^{-2}	95	~30
$(TaSe_4)_2I$	0.12	139	~65
$(NbSe_4)_{10}I_3$	0.17	197	~60

I-V curve to a Zener-type expression in order to extract a value for E_0 that is more representative of the average depinning field.

The basic shape of the dc I-V curve for sliding CDW materials under most experimental conditions is very distinctive. Above threshold, the CDW conductance follows the functional form $\exp(-E_0/E)$, as indicated in Eq. (1.1). This form is, of course, reminiscent of the Zener-type tunneling which occurs in semiconductors. In most cases, the experimental data can be reasonably fitted by the approximate expression

$$I_{\rm CDW}(E)\approx G_b(E-E_T)e^{-E_0/E}, \tag{6.13}$$

where $E_T<E_0$. An alternative form with E replaced by $E-E_T$ in the exponential factor was proposed several years ago by Fleming,[4] who obtained very accurate fits in this manner to his experimental data on $NbSe_3$ as shown in Fig. 1. The precision of the fit to a Zener form is further illustrated in Fig. 11, using some of our recent data on $NbSe_3$ superposed for five different temperatures on the upper CDW transition. The measured values of $I_{CDW}(E)/G_bE$ are seen to depart from the universal curve $\exp(-E_0/E)$ only in the immediate neighborhood of threshold, and to very precisely follow this simple form over 2 orders of magnitude in the applied electric field.

For strong pinning, the simple Zener form of the dc I-V curve was explained several years ago by Portis.[60] His argument requires only a minor reinterpretation within the present context. If we return to Eq. (6.7), the average depinning field is given by the condition $eE_0L\approx\gamma(\Delta/4)$. The distribution in the lengths l between successive impurities about the average value L is given in Eq. (5.3). If each segment on every chain could move independently, an electric field E would depin only those segments longer than $l_{\rm min}=(E_0/E)L$. The conductance under these conditions would thus be proportional to

$$\int_{l_{\rm min}}^{\infty} dl\frac{1}{L}e^{-l/L}=e^{-E_0/E}. \tag{6.14}$$

Of course, each segment on every chain cannot depin individually. The acceleration of a large phase-coherent volume containing a great many strong impurities should, however, still be roughly proportional to the fraction of individual segments which would conduct if they could move separately. The dc CDW current thus assumes the approximate form given in Eq. (6.13). According to this argument, we should expect that the threshold field E_T is essentially equal to the characteristic field E_0. This value is indeed approached in the best $NbSe_3$ samples under optimum experimental conditions. But in most cases, E_T is found to be considerably less than E_0, presumably due to inhomogeneities in the impurity distributions and electric fields within the crystals. Values of E_0 extracted from fits to Eq. (6.13), therefore, represent the most reliable experimental measure of the average electric field needed in order to depin the CDW.

In his early work on $NbSe_3$, Fleming[4] was able to determine accurate values for $E_0(T)$ at several temperatures on the upper transition, in addition to the temperature dependence of the threshold field E_T for both CDW's. His results are reproduced in Fig. 12. The rapid increase in $E_0(T)$ seen as the temperature is reduced below 100 K can be accurately fitted by

$$E_0^{\rm expt}(T)\approx(1.8\ {\rm V/cm})e^{-T/(36\ {\rm K})}. \tag{6.15}$$

Using the estimate $\Delta\approx3.9\times10^{-2}$ eV given in Table I, together with the representative value $L\approx2.3$ μm obtained in Sec. III, the theoretical predictions of Eqs. (6.9)–(6.11) for the upper $(NbSe_3)^{\rm I}$ CDW become

$$E_0^{\rm theor}(T)\approx(2.2\ {\rm V/cm})e^{-T/(45\ {\rm K})}. \tag{6.16}$$

The quantitative agreement seen here is quite remarkable in view of our many approximations.

Turning now to orthorhombic TaS_3, we should like to

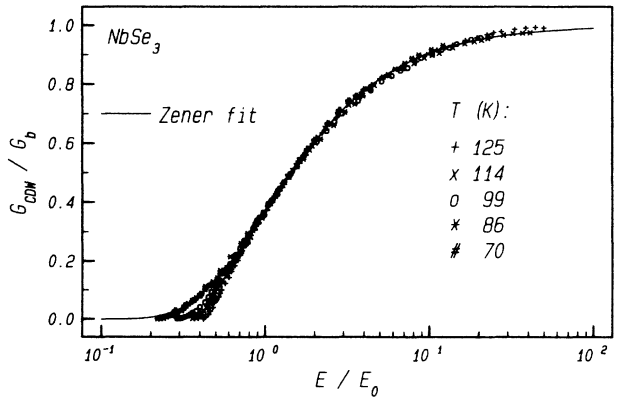

FIG. 11. Normalized nonlinear dc-conductance data as a function of electric field for a crystal of $NbSe_3$, superposed for five different temperatures on the upper CDW transition. The solid curve represents the Zener form $\exp(-E_0/E)$.

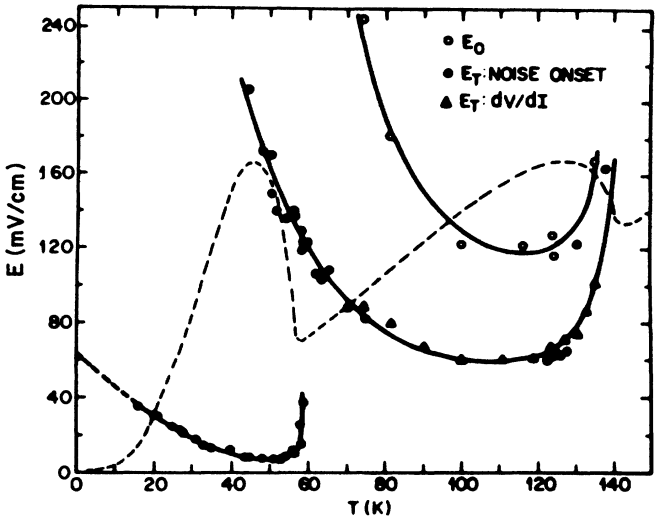

FIG. 12. Characteristic depinning field E_0 for the upper CDW state of $NbSe_3$, and measured threshold fields E_T for both upper and lower CDW states, as functions of temperature. Dashed curve shows relative magnitude of the low-field dc resistivity, indicating the two CDW transitions at $T_p^1=145$ K and $T_p^2=59$ K. Reproduced from Fleming (Ref. 4).

see how the experimental values of E_T listed for the intentionally doped crystals in Table II compare with the predictions of the theory. Using $\Delta \approx 6.0 \times 10^{-2}$ eV and the values for L estimated from the experimental dielectric constants yields the theoretical results for E_0 quoted in Table II. The comparison is seen to be very good, although it should be noted that $E_0 \approx 3E_T$ for typical o-TaS_3 crystals at this temperature. Nevertheless, the theoretical estimates seem generally accurate, although they appear to rise a bit too slowly with decreasing L, particularly in the case of the 0.2% Nb crystal. This behavior is, however, in qualitative accord with the discussion given in conjunction with our estimate for γ in Eq. (6.8). For values of $L \lesssim 0.3$ μm or $n_i \gtrsim 0.1\%$ we indeed expect a larger E_0, since the average phase $\bar{\phi}(r)$ should become significantly interpolated toward the pinned value ϕ_0^i at each impurity site, causing our estimate of $\gamma \approx 1/(N_i)^{1/2}$ to be too small.

To check the temperature dependence of $E_0(T)$ for orthorhombic TaS_3, we can utilize some of our previously published data.[61] Five quoted values for E_0 covering the temperature range $154 < T < 209$ K above the apparent commensurate transition near 140 K can be accurately fitted by

$$E_0^{\text{expt}}(T) \approx (34 \text{ V/cm}) e^{-T/(63 \text{ K})} . \quad (6.17)$$

Using the value $L \approx 1.3$ μm obtained in Table II as representative of nominally pure o-TaS_3, the prediction of Eqs. (6.9)–(6.11) becomes

$$E_0^{\text{theor}}(T) \approx (7.5 \text{ V/cm}) e^{-T/(70 \text{ K})} , \quad (6.18)$$

in reasonable agreement with experiment. We note that E_0 rises abruptly with decreasing temperature over this range, although the threshold field E_T is often observed to be relatively constant as seen in Fig. 10. This observation again indicates the importance of using E_0 rather than E_T to characterize the average depinning field.

The importance of measuring E_0 is further underscored by our recent dc data on $(TaSe_4)_2I$ shown in Fig. 13. The initial CDW motion is observed above a threshold field $E_T \approx 1$ V/cm nearly independent of temperature as in the data of Cava *et al.*[48] On the other hand, E_0 is seen to rise sharply with decreasing temperature in qualitative agreement with the E_T data of Monceau[33] shown in Fig. 10. The experimental values for E_0 in Fig. 13 are accurately fitted by

$$E_0^{\text{expt}}(T) \approx (94 \text{ V/cm}) e^{-T/(112 \text{ K})} . \quad (6.19)$$

The phase correlation length L can be estimated using the value $\bar{\omega}_p/2\pi \approx 4.6$ GHz obtained in Sec. V, together with the parameter estimates given in Table I which yield $c_0 \approx 4.9 \times 10^5$ cm s^{-1}. Inserting these values into Eq. (3.10) gives $L \approx 0.5$ μm. The theoretical prediction for the average depinning field then becomes

$$E_0^{\text{theor}}(T) \approx (53 \text{ V/cm}) e^{-T/(139 \text{ K})} , \quad (6.20)$$

again in good agreement with experiment.

The theory of strong pinning and phase slip that we propose here easily accounts for the functional form of the dc I-V curve seen under most experimental conditions, as well as for the characteristic temperature dependence of the threshold field shown in Fig. 10. Estimates for the average depinning field $E_0(T)$ are found to be in excellent quantitative agreement with experimental data on $NbSe_3$, o-TaS_3, and $(TaSe_4)_2I$. The variation of E_0 with impurity concentration shown in Table II also appears generally correct, with some understandable deviation at the highest doping level caused by an inadequacy in our approximations for $L \lesssim 0.3$ μm. The range and quality of the correspondence between the theory and available experimental data on dc motion is thus very substantial.

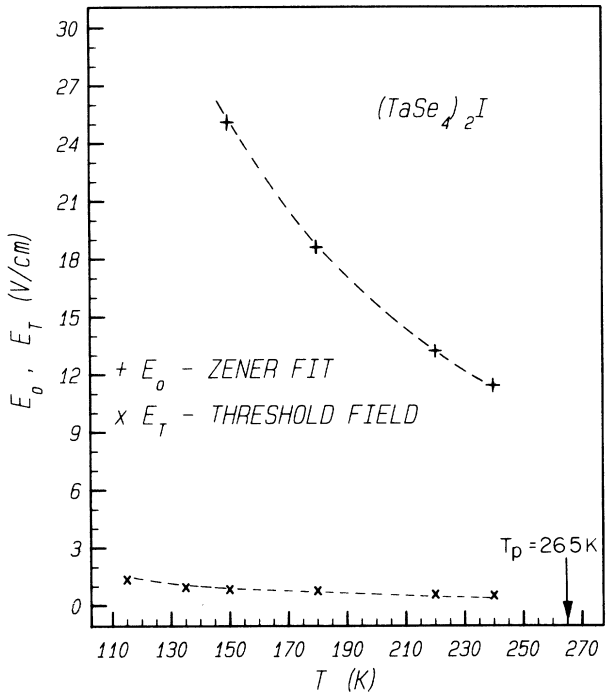

FIG. 13. Characteristic depinning field E_0 and minimum threshold field E_T for a crystal of $(TaSe_4)_2I$ as a function of temperature. Dashed lines are guides to the eye.

VII. CURRENT OSCILLATIONS

According to the present theory, dc CDW motion occurs by means of phase slip. Far above threshold, where the drift velocity is nearly constant, small current oscillations are produced by the CDW's motion over an effective pinning potential of the general form illustrated in Fig. 9. Close to threshold, however, the dc motion is composed of discrete "jumps" which rapidly advance the phase by 2π within each phase-coherent volume, producing many harmonics in the narrow-band noise spectrum. When phase slip occurs within a particular region, the time scale for transient readjustment of the phase configuration is given by the dielectric relaxation frequency, as discussed in Sec. IV. For average CDW drift frequencies $\omega_d = d\bar{\phi}/dt$ small compared to the dielectric relaxation frequency ω_0, we should thus expect to observe a locally "jerky" motion consisting of discrete periodic

pulses with a duration $\sim 1/\omega_0$.

The results of this behavior are readily apparent in experimental measurements of the narrow-band noise. In our recently published data on $NbSe_3$,[30] the magnitude and harmonic content of the current oscillations may be seen to become effectively independent of electric field for applied dc voltages $V \gtrsim 5V_T$, as shown in Fig. 14. At these dc voltages, the fundamental drift frequency exceeds the dielectric relaxation frequency $\omega_0/2\pi \approx 5$ MHz. In this high-field regime, we demonstrated that the current oscillations and the mode locking to external ac signals could be quantitatively reproduced by a simple model based on overdamped motion in a nonsinusoidal effective pinning potential. The form for the effective potential used in that analysis consisted of intersecting cosine curves, very similar to the intersecting parabolas shown in Fig. 9, and the experimental data indicate that the actual periodic potential is slightly more rounded. From the widths of the current steps induced onto the dc I-V curve by mode locking, we found that the maximum restoring force associated with this periodic pinning potential corresponds to at least one-third of the threshold field in good crystals, as shown in Fig. 15 for ac frequencies $\gtrsim 5$ MHz.

This simple behavior seen in our experiments at high fields and frequencies is dramatically altered for $V < 5V_T$, when the fundamental drift frequency ω_d becomes smaller than ω_0. In this regime, the harmonic content of the current oscillations increases rapidly and the magnitude of the fundamental falls off. The number of measurable harmonics is approximately given by $\sim 2\omega_0/\omega_d$, as would be expected if the dc motion consists of jumps of duration $\sim 1/\omega_0$. The maximum widths of the mode-locked steps are also seen to decrease rapidly in Fig. 15 when the fundamental drift frequency becomes less than $\omega_0/2\pi \approx 5$ MHz.

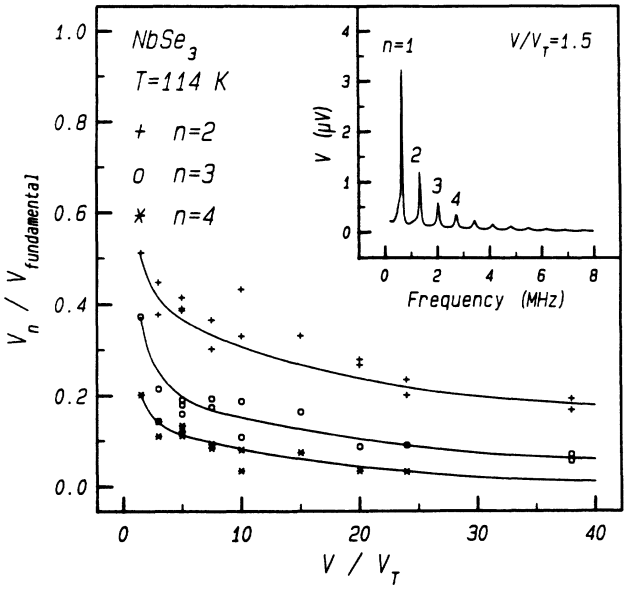

FIG. 14. Amplitudes of the first three harmonics of the current oscillation spectrum in $NbSe_3$ at 114 K normalized by that of the fundamental. Significant harmonic content remains even at very high fields. Solid lines are guides to the eye. Reproduced from Thorne *et al.* (Ref. 30).

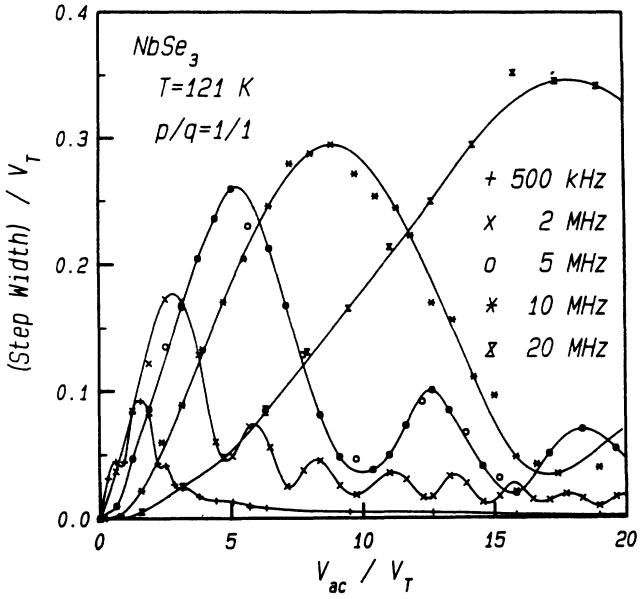

FIG. 15. Width of the fundamental mode-locked step on the dc I-V curve vs applied ac amplitude at several frequencies. The periods of the oscillations with ac amplitude are roughly proportional to the ac frequency. The maximum width of the steps increases at low frequencies but saturates at high frequencies. Solid lines are guides to the eye. Reproduced from Thorne *et al.* (Ref. 30).

The same picture emerges even more vividly from the NMR experiments of Ross, Wang, and Slichter.[44] We have already discussed their result $\delta\bar{\phi} \approx 2°$ for the average angular displacement in a dc electric field $E \approx 0.75E_T$ just below the conduction threshold for the upper $NbSe_3$ CDW. In Sec. III, we showed that this surprisingly small average displacement is actually in very good agreement with our simple model for CDW polarization. The fact that the displacement remains so small near threshold ultimately results from local thermal fluctuations, which greatly reduce the magnitude of the depinning field according to Eqs. (6.10) and (6.11).

In order to characterize the CDW's motion, Ross *et al.* performed a further series of NMR experiments on their aligned sample, composed of 30 crystals each 1 cm in length, but this time biased above the average conduction threshold ~ 200 mV/cm at 77 K. These results are more completely described by Ross,[62] where the average drift frequencies are inferred directly from narrow-band noise measurements rather than by the calculated estimate contained in the published paper.[44] One set of experiments observed saturation in the nuclear magnetization as a result of rapid CDW motion. This effect occurs when significant components of the CDW motion spectrum reach the NMR frequency, 88 MHz in this case, inducing transitions between the Zeeman levels. The saturation onset was observed to occur when the fundamental CDW noise peak reached about one-half this frequency,

near 45 MHz. Their analysis indicates that the observed behavior can be consistently explained by the presence of a second harmonic in the motion spectrum with a relative amplitude of $\sim 5\%$ of the fundamental. This result is similar to, but somewhat less than, the observation in Fig. 14 of a second harmonic of relative amplitude $\sim 20\%$ in the current oscillations at a higher temperature where the CDW motion is more coherent. Analysis of the NMR line shape yielded a similar estimate of $\sim 4\%$ for the second-harmonic amplitude. Ross[62] therefore concludes that the CDW motion, while noticeably nonsinusoidal, is relatively smooth at fields greater than ~ 7 times the conduction threshold.

The motional-narrowing results obtained by Ross *et al.*[44] closer to threshold, however, paint an entirely different picture. The random positions of the Nb nuclei with respect to the incommensurate CDW charge distribution produces a static broadening $\Delta\omega/2\pi \approx 30$ kHz of the NMR line shape for the chains containing the CDW, as indicated in Fig. 16. Ordinarily, motional narrowing would be expected when the CDW drift frequency ω_d exceeds $\Delta\omega$, so that each nucleus rapidly samples an average charge distribution over the time scale $\sim 1/\Delta\omega$ needed to resolve the static broadening. Motional narrowing is seen in Fig. 16, but not until the drift frequency (as measured by the narrow-band noise fundamental) reaches $\omega_d/2\pi \approx 15$ MHz near 0.7 V/cm. The narrowing of the NMR linewidth seen here is rather abrupt. At 0.55 V/cm the linewidth essentially equals its static value, while at 0.70 V/cm it is reduced by half. A Fourier transform of the echoes obtained at 1.4 V/cm showed complete motional narrowing, with no remaining trace of the static line shape. Several independent NMR experiments also indicate that CDW motion is reasonably uniform throughout their multicrystal sample. The results shown in Fig. 16 are thus an accurate reflection of the local motion seen by each Nb nucleus as the CDW is depinned above threshold.

This remarkable increase of ~ 500 in the motional-narrowing onset frequency for $NbSe_3$ was considered in detail by Ross. He concluded[63] that it could only be explained if, as illustrated in Fig. 17, "the CDW can be considered to move as a sequence of steps, at voltages just above threshold. If each step advances the CDW phase by exactly 2π, then the NMR frequency shift, which is periodic in the CDW phase, will be the same before and after the step. During the actual step, the frequency shift will execute one cycle through the frequency extremes of the line shape, but between the steps the frequency shift will be steady at a locally-defined value." Under these conditions, motional narrowing would not be expected until the spacing between the steps becomes comparable to the average step width. Since motional narrowing was observed at $\omega_d/2\pi \approx 15$ MHz, Ross inferred that the duration of a single current step must be $\sim 0.1\ \mu$s.

We now recognize this step width as essentially the dielectric relaxation time for $NbSe_3$. It seems to us that motional narrowing of the NMR line shape could only be forestalled to CDW drift frequencies ~ 500 times in excess of the static broadening if the effect of each step was to displace the CDW phase by *exactly* 2π. This, in turn, is only plausible if the dc motion proceeds by phase slip. Indeed, the description of CDW motion near threshold that Ross provides is precisely what one would expect on this basis.

Janossy *et al.*[64] have recently published an NMR study of motional narrowing in $Rb_{0.3}MoO_3$ for $40 < T < 60$ K that appears to show a dramatically different result. Their data are reproduced in Fig. 18. The narrowing is seen to take place at a drift frequency $\omega_d/2\pi \approx 5$ kHz comparable to the static line broadening $\Delta\omega/2\pi \approx 10$ kHz, and a factor of $\sim 10^3$ smaller than the narrowing frequency in $NbSe_3$. In these experiments, the electric field $E \approx 15E_T$ is held constant, and the CDW drift velocity is rapidly altered by changing the temperature.

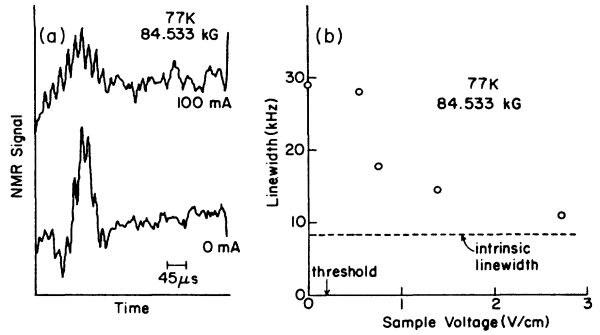

FIG. 16. (a) Spin echoes in $NbSe_3$ at 77 K illustrating current-driven motional narrowing of the Nb NMR line for the "yellow" chain containing the CDW. The broader echo implies a narrower line. (b) Dependence of the linewidth on dc bias voltage applied across the 1-cm sample. The intrinsic width is that of the "red" and "orange" Nb sites which do not contain the CDW. Reproduced from Ross *et al.* (Ref. 44).

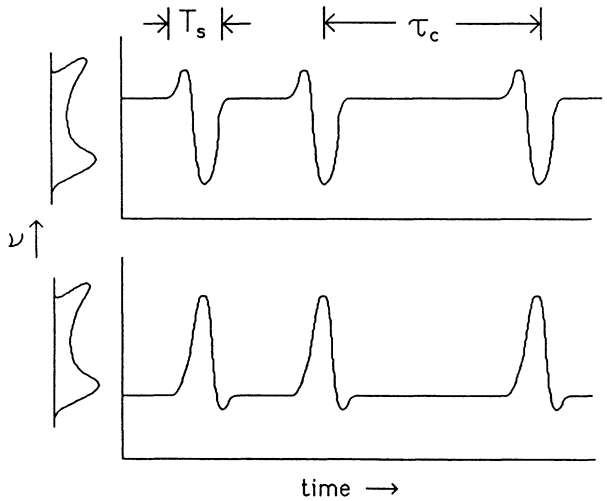

FIG. 17. The stepped motion, as proposed for small CDW velocities. Illustrated is the NMR frequency vs time for nuclei at two different points in the static line shape, indicated schematically at the left of each graph. Reproduced from Ross (Ref. 62).

This result can be readily understood within the context of our model. In the high-field limit $\omega_d \gg \omega_0$, where the current pulses in Fig. 17 run together, the CDW motion will become relatively smooth with a fundamental drift frequency:[47]

$$\omega_d \approx \omega_0 (E/E_T) \quad \text{for } E \gg E_T \ . \tag{7.1}$$

The behavior here is similar to that of a relaxation oscillator at applied voltages far in excess of the breakdown. The dielectric relaxation frequency as a function of temperature can be estimated from the experimental results quoted in Eq. (4.15) for the nearly identical material $K_{0.3}MoO_3$. Use of the resulting values together with $E/E_T = 15$ in Eq. (7.1) then reproduces the average CDW drift frequencies shown in Fig. 18 to within a factor of 2.

Over the temperature range $40 < T < 60$ K of the experiments of Janossy *et al.*, the dielectric relaxation frequency remains smaller than the static line broadening $\Delta\omega/2\pi \approx 10$ kHz, with $\omega_0/2\pi \approx 2.6$ kHz at the highest temperature $T = 59.2$ K shown in Fig. 18. Under these conditions, the motional narrowing should occur when $\omega_d \sim \Delta\omega$, as observed here for $\omega_d/2\pi \approx 5$ kHz at $T = 49.3$ K. The very different behavior seen in $Rb_{0.3}MoO_3$ compared to $NbSe_3$ results from the tremendous reduction in the dielectric relaxation frequency due to restricted normal carrier screening, as discussed in Sec. IV.

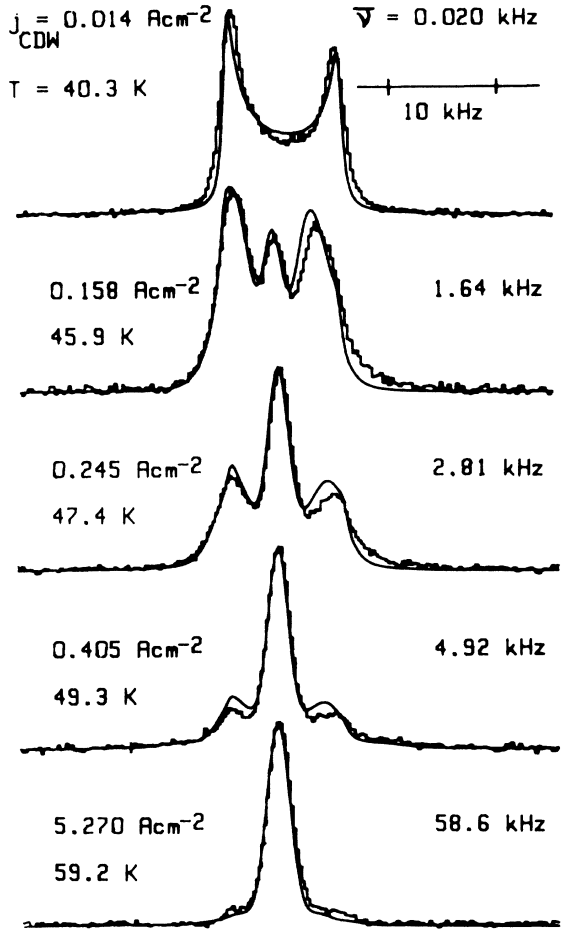

FIG. 18. NMR line shape in $Rb_{0.3}MoO_3$ as a function of CDW current density for $40 < T < 60$ K. The field is fixed at $E = 1.5$ V/cm ($\approx 15E_T$) and the temperature is varied to change j_{CDW}. Solid lines are computer-fitted curves using a relative CDW velocity distribution inferred from the narrow-band noise and the average drift frequencies $\bar{v}$ shown at the right for each temperature, in good agreement with their measured values. Reproduced from Janossy *et al.* (Ref. 64).

According to our interpretation, the motional-narrowing frequency in $Rb_{0.3}MoO_3$ should change dramatically for slightly higher temperatures $T > 65$ K, where Eq. (4.15) predicts that $\omega_0 > \Delta\omega$. In this region, $Rb_{0.3}MoO_3$ is expected to display motional narrowing at a CDW drift frequency $\omega_d \sim \omega_0$ that increases very rapidly with temperature. Thus by simply adjusting the temperature, it should be possible to show that $Rb_{0.3}MoO_3$ can display the same remarkable behavior seen in $NbSe_3$.

Previously published data on $Rb_{0.3}MoO_3$ by Segransan *et al.*[65] at $T = 77$ K appear to confirm this prediction. At 77 K, Eq. (4.15) yields a dielectric relaxation frequency $\omega_0/2\pi \approx 67$ kHz. Motional narrowing is observed at a drift frequency $\omega_d/2\pi \approx 70$ kHz close to the expected value, and much larger than the narrowing frequency ~ 5 kHz seen at 49.3 K in Fig. 18. An earlier NMR study of $Rb_{0.3}MoO_3$ at $T = 77$ K by Douglass *et al.*[66] failed to produce evidence for motional narrowing at current densities up to 0.45 A/cm^2. According to later measurements by Janossy *et al.*[64] this current density translates into an average CDW drift frequency $\omega_d/2\pi \approx 6$ kHz, too small to observe the motional narrowing at 77 K by an order of magnitude.

All available NMR evidence on motional narrowing in *both* $NbSe_3$ and $Rb_{0.3}MoO_3$ is thus accurately and quantitatively described by the present model. Further experiments are needed on $Rb_{0.3}MoO_3$, however, in order to unambiguously confirm that the narrowing frequency follows the dielectric relaxation frequency for $T > 65$ K. By sampling the *local* CDW motion at nuclear sites throughout the sample, NMR techniques are capable of providing critical information on CDW dynamics that is difficult or impossible to obtain through electrical measurements alone.

Further direct experimental evidence in favor of phase slip comes from an effect that has been called "pulse-duration memory" by Fleming and Schneemeyer,[67] who were the first to characterize it in $K_{0.3}MoO_3$. Figure 19 reproduces data of Ido *et al.*[68] illustrating this phenomenon in a small and especially coherent $NbSe_3$ crystal. A series of identical current pulses is applied to the sample just above the CDW conduction threshold, and the resulting excess conductivity σ_e due to CDW motion is plotted as a function of time. Figure 19 shows the behavior observed when the duration of the current pulses is gradually increased. The oscillations in σ_e always end at the maximum value, regardless of the pulse width, as if the phase were locked to the end of the pulse. The number of oscillations in σ_e is always observed to be integral. With increasing pulse width, the oscillation period gradually lengthens until the number of oscillations suddenly jumps by one complete cycle. Ido *et al.*

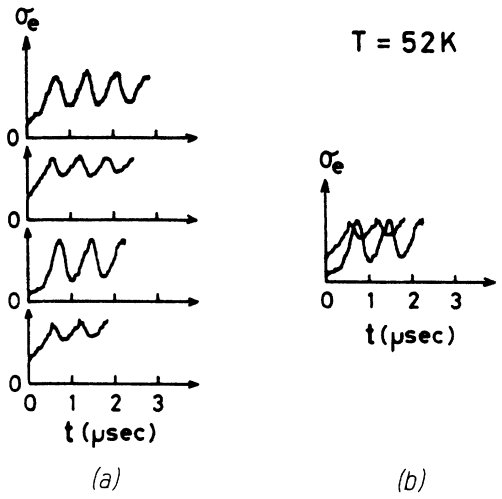

FIG. 19. (a) Extra conductance σ_e of a $NbSe_3$ crystal due to periodic CDW motion as a function of time. A constant electric field $E \sim 1.4E_T$ is applied in a series of pulses, and the results are shown here for several different values of the pulse width. (b) Comparison between the extra CDW conductances observed for two values of pulse width having the same number of oscillations. Reproduced from Ido *et al.* (Ref. 68).

show that as the pulse width is increased, the modulation of σ_e also increases in a manner which yields a constant value for the time integral of the CDW current, so long as the total number of oscillations remains constant. By converting the integrated current to a spatial displacement, they found that the CDW moves ahead by precisely $m\lambda_{CDW}$ during each current pulse, where m is the number of cycles observed in σ_e. They conclude that this behavior must be associated with depinning of the CDW by phase slip at strong pinning centers.

A very wide range of experimental evidence on current oscillations thus supports the idea of dc CDW motion by phase slip. Of all these results, the most compelling are those of Ross *et al.*[44,62] on motional narrowing of the $NbSe_3$ NMR linewidth, which may prove impossible to explain on any other basis. Simulations by Littlewood[25] using a one-dimensional version of the classical phase-only model of deformable CDW's indicate that the phase tends to advance relatively rapidly through large fractions of 2π in alternating spatial regions as time progresses. The local jumps within this model, however, are not nearly precise enough to account for the experimental NMR data on motional narrowing. Only a phase-slip process, we believe, can ensure the exact local registration of the CDW over the intervals necessary to forestall the motional narrowing to drift frequencies ~ 500 times in excess of the static line broadening. Furthermore, all other experimental evidence on the current oscillation phenomena appears to be in detailed and consistent agreement with this point of view.

VIII. CONCLUSION

In this paper, we have presented a theory for CDW dynamics based on the idea that the phase is strongly pinned at each impurity site, and that dc motion is made possible only by phase slip. The theory thus breaks with the conventional wisdom of the past several years, in which CDW dynamics was considered to result primarily from weak impurity pinning. The present model is based on a modified version of the three-dimensional Ginzburg-Landau analysis of strong pinning given by Lee and Rice[11] many years ago. The major conceptual step we have taken here is to demonstrate that strong pinning does not limit the phase coherence in CDW systems to the average volume of a single impurity, at least for the relatively dilute concentrations present in nominally pure crystals. No attempt has been made to go beyond the Ginzburg-Landau analysis toward a more microscopic formulation of the CDW's interaction with individual impurities. Tütto and Zawadowski[69] have provided an elegant microscopic picture of CDW pinning, however, which we believe could potentially be applied to characterize the phase-slip process.

Most of the phase gradients needed to interpolate between the average $\bar{\phi}(r)$ and the pinned value ϕ_0^i at a particular impurity site are estimated to be confined to a tiny region ~ 75 Å in length and effectively one chain in cross-sectional area. Because of this, the phase coherence distance along the chain direction is expected to be comparable to the average impurity spacing. The average phase $\bar{\phi}(r)$ is expected to be transversely correlated over a relatively large total volume, containing up to a few hundred individual impurities in good $NbSe_3$ crystals.

The minimum interaction energy between a single impurity and the CDW that is needed in order to strongly pin the phase is estimated to be $\sim 10^{-2}$ eV. Thus we expect that most types of impurities will act as strong-pinning centers, whether they are charged or not, in relatively dilute concentrations. The original doping study carried out on $NbSe_3$ by Brill *et al.*[70] indicated that the nonisolectronic impurity Ti causes a much larger increase in the threshold field than Ta, which is isolectronic to Nb. On the other hand, these authors were unable to obtain a smooth correlation of their dc data with the nominal amount of Ti doping. A similar and more recent doping study is reported in the paper by Ido *et al.*[68] Here the effects of Ti and Ta impurities on the measured threshold fields are seen to be very comparable, although there are some apparent differences noted in the shapes of the dc I-V curves. Furthermore, the data of Brill *et al.* which indicate that both E_T and E_0 increase approximately as the square of the Ta concentration is not in serious conflict with the present model of strong pinning. The theoretical estimate given in Eq. (6.9) is seen to be proportional to $n_i^{4/3}$, but the depinning field is expected to rise faster with impurity concentration when $L < 0.3$ μm or $n_i > 1000$ ppm. The nominal Ta concentration for most of the samples measured by Brill *et al.* falls within this range, so that the case for weak pinning on the basis of these experiments is by no means clearcut. While further doping studies will certainly be important to testing the present theory, the currently available data appear to be reasonably consistent with this revised view of strong pinning.

The ideas of strong pinning and phase slip have been

developed throughout this paper in order to characterize most of the major aspects of CDW dynamics that have been so intensively studied over the past ten years. During the course of this work, we have continually been amazed and gratified by the close quantitative correspondences that have emerged between our relatively simple estimates and the experimental data. Having come this far, we are now convinced that the basic concepts of this theory must be fundamentally correct.

We have also come to understand how the behavior that we previously considered as evidence for quantum tunneling can emerge from the present picture. The Zener-like form of the dc I-V curve results quite naturally from strong pinning, as argued by Portis[60] several years ago. The corresponding shape of the ac conductivity in overdamped systems is due to the distribution in pinning frequencies given by Eq. (5.4), which is essentially identical to a result previously obtained for strong pinning in one dimension by Fukuyama and Lee.[12] The nonlinear mixing experiments that we have performed[19,20] were required to fit the photon-assisted tunneling predictions at the lowest frequencies, since in this regime the theoretical expressions reduce to the classical derivatives of the dc I-V curve. At high frequencies, the nonlinear response must vanish because the CDW no longer feels the effects of impurity pinning. By scaling the ac and dc responses, we were thus able to obtain an interpolation between these two extremes that corresponded rather well to the experimental data. Recently, Liu and Sneddon[71] have shown that qualitatively similar results can be obtained from a classical Frenkel-Kontorova model in which the effective pinning potential remains constant at arbitrary dc electric fields, in contrast to the Sneddon, Cross, and Fisher[21] model of deformable CDW's. The internal phase shift that they predict for harmonic mixing is surprisingly small within the region of experimental interest, and roughly comparable to the uncertainty in our measurements. This apparent lack of any internal phase shift for harmonic mixing was previously interpreted[19,20] by us as strong evidence in favor of the tunneling hypothesis.

The problem of explaining the observed behavior of CDW systems has baffled a large number of people for a very long time. If the present theory is correct, this long delay in achieving a satisfactory interpretation of CDW dynamics is the result of (1) a misunderstanding of the large-scale phase coherence properties for a strongly pinned system, and (2) a concentration on phase-only models, in which the possibility of extremely strong pinning and phase slip is *a priori* excluded.

ACKNOWLEDGMENTS

Throughout the course of our work on charge-density-wave systems, we have benefited greatly from collaborations with our colleagues J. H. Miller, Jr., and J. W. Lyding. We thank L. Mihaly for a seminal discussion on CDW polarization, which led us to formulate our ideas in terms of Eq. (3.5), and both C. P. Slichter and J. H. Ross, Jr., for explanations of their NMR experiments on $NbSe_3$. This work was supported by the U.S. Joint Services Electronics Program (under Contract No. N00014-84-C-0149) and by the National Science Foundation (under Grant No. NSF-DMR-86-12860).

APPENDIX A

Mean-field theory predicts a Peierls transition temperature given by the BCS expression

$$T_p^{\mathrm{MF}}=\Delta/1.76k_B \ . \tag{A1}$$

In a truly one-dimensional system, however, thermal fluctuations would completely suppress the phase transition to $T=0$. The data collected by Monceau[72] show that $2\Delta/k_BT_p\approx 12$ for most sliding CDW materials, so the Peierls temperature $T_p\approx 0.3T_p^{\mathrm{MF}}$ is indeed substantially depressed below the mean-field value. The magnitude of this depression can therefore be used to infer the anisotropy of the electronic structure for these systems.

Horovitz, Gutfreund, and Weger[73] consider a model with the following band structure:

$$\varepsilon(k)=\varepsilon_z(k_z)-\eta\varepsilon_0[\cos(k_x a_\perp)+\cos(k_y a_\perp)] \ . \tag{A2}$$

The Fermi surface lies at $\varepsilon(\mathbf{k})=0$, and the average value of k_F along the chain direction is determined by $\varepsilon_z(k_F)=0$. The longitudinal Fermi velocity is then $v_F=\hbar^{-1}d\varepsilon_z(k)/dk\mid_{k=k_F}$. The energy scale ε_0 is defined to be $\varepsilon_0=\hbar v_F k_F/2$, which is equal to the Fermi energy if $\varepsilon_z(k)=\hbar^2k^2/2m$. The dimensionless parameter η is then a measure of the anisotropy. An explicit form for $\varepsilon_z(k)$ need not be specified, since for $\eta\ll 1$ the properties of the model depend only on the dispersion near the Fermi surface.

Horovitz *et al.* express their results in terms of the parameter

$$\tau=\frac{k_BT_p^{\mathrm{MF}}}{\varepsilon_0}=\frac{\Delta}{1.76\varepsilon_0} \ . \tag{A3}$$

They find that a Peierls transition is possible only for

$$\eta<\eta_c\approx 3.5(\tau/\alpha)^{1/2} \ . \tag{A4}$$

Here $\alpha\propto d^2\varepsilon_z/dk^2\mid_{k=k_F}$, with $\alpha=1$ for free-electron propagation and $\alpha=\pi/4$ for a $\frac{1}{4}$-filled tight-binding band. For $\eta>\eta_c$, the band structure is no longer sufficiently one dimensional to produce the phase transition.

In the regime of strong one-dimensional fluctuations, where $T_p<0.5T_p^{\mathrm{MF}}$, the suppression of the Peierls temperature is predicted to be

$$T_p\approx T_p^{\mathrm{MF}}\exp(-2.5\tau/\eta) \ . \tag{A5}$$

For the sliding CDW materials with $T_p\approx 0.3T_p^{\mathrm{MF}}$, this gives

$$\eta\approx 2\tau\approx\frac{\Delta}{\varepsilon_0} \ . \tag{A6}$$

The value of ε_0 equals the Fermi energy ε_F for a free-electron band, and $\varepsilon_0=(\pi/16\sqrt{2})W_\parallel$ for a $\frac{1}{4}$-filled tight-binding band. Mean-field theories predict that $\Delta\approx 4\varepsilon_F e^{-1/\lambda}$, where λ is the dimensionless electron-phonon coupling constant for $Q=2k_F$. Equation (A6)

therefore indicates that η should be roughly material independent, assuming that λ is similar for all sliding CDW crystals. We estimate its numerical value for orthorhombic TaS_3 by taking $\Delta \approx 0.06$ eV and $\varepsilon_0 \approx 0.4$ eV ($W_\parallel \approx 3$ eV), so that

$$\eta \approx 0.15 . \tag{A7}$$

This estimate is nearly an order of magnitude greater than the values $\eta \approx 0.02$ inferred by Carneiro[74] for the $Pt(CN)_4$ salts, reflecting the much more three-dimensional nature of the sliding CDW materials. Note that our estimates for TaS_3 imply a transverse bandwidth $W_\perp \approx 0.12$ eV. In this case $W_\perp \approx 2\Delta$, and a larger value of η than the estimate of Eq. (A7) would probably preclude a complete metal-insulator transition.

Horovitz *et al.* find that the transverse-to-longitudinal coherence-length ratio is given by

$$\frac{\xi_\perp}{\xi_\parallel} = \frac{1}{2\sqrt{2}} \eta k_F a_\perp . \tag{A8}$$

Using $k_F a_\parallel \approx \pi/4$ and $a_\perp / a_\parallel \approx 2$ then yields the following result for the sliding CDW materials:

$$\xi_\perp \approx 0.08 \xi_\parallel . \tag{A9}$$

APPENDIX B

The elastic energy that would be required to smoothly interpolate the CDW phase between strong-pinning centers may be estimated using Eq. (2.11). Constraining the volume of the phase variation to the average volume per impurity, $AL = A_0 \bar{L}$, gives

$$F(\nabla\psi) \approx f_0 \left[2\xi_\perp^2 L + \xi_\parallel^2 \frac{A_0 \bar{L}}{L^2} \right] (\bar{\phi} - \phi_0)^2 . \tag{B1}$$

Minimizing with respect to L then yields the optimum dimensions

$$\begin{aligned} L_{\min} &= \left[\frac{\xi_\parallel}{\xi_\perp} \right]^{2/3} (A_0 \bar{L})^{1/3} , \\ A_{\min} &= \left[\frac{\xi_\perp}{\xi_\parallel} \right]^{2/3} (A_0 \bar{L})^{2/3} . \end{aligned} \tag{B2}$$

The ratio $L_{\min}/(A_{\min})^{1/2} = \xi_\parallel / \xi_\perp$, exactly as would be obtained from the rescaled version of the Lee and Rice[11] free energy. Taking $\xi_\perp \approx 0.08 \xi_\parallel$ and $A_0 \approx 70$ Å^2, the numerical values are given by

$$\begin{aligned} L_{\min} &\approx (500 \text{ Å}) [\bar{L}(\mu\text{m})]^{1/3} , \\ A_{\min} &\approx (20 A_0) [\bar{L}(\mu\text{m})]^{2/3} . \end{aligned} \tag{B3}$$

Inserting the results of Eq. (B2) back into Eq. (B1) produces the following estimate for the elastic energy per impurity required for a smooth interpolation of the phase:

$$E_{\text{elast}} \approx 3 f_0 \left[\frac{\xi_\parallel}{\xi_\perp} \right]^{2/3} \xi_\perp^2 (A_0 \bar{L})^{1/3} (\bar{\phi} - \phi_0)^2 . \tag{B4}$$

In terms of Eq. (2.13) for the energy E_{pin} needed to individually adjust the phase to a uniform $\bar{\phi}$, we find

$$\frac{E_{\text{elast}}}{E_{\text{pin}}} \approx \frac{3\sqrt{2}}{4} \left[\frac{\xi_\perp}{\xi_\parallel} \right]^{1/3} \frac{\bar{L}^{1/3}}{A_0^{1/6}} \approx 4.9 [\bar{L}(\mu\text{m})]^{1/3} . \tag{B5}$$

We note that this ratio is extremely insensitive to our numerical estimates for $\xi_\perp / \xi_\parallel$ and A_0.

APPENDIX C

Maki[59] has proposed a model for incorporating thermal fluctuations of the CDW phase in calculating the dc threshold field. His basic argument can be considerably simplified within the present context.

For a CDW with a periodic pinning potential of the form $V(\phi) = -V_{\max} \cos\phi$, the equilibrium configuration at $T = 0$ is the state of lowest energy $\phi = 0$. At finite temperatures, thermal fluctuations will produce a distribution

$$P(\phi) = \frac{1}{(2\pi \langle \phi^2 \rangle)^{1/2}} e^{-\phi^2 / 2\langle \phi^2 \rangle} , \tag{C1}$$

where

$$V_{\max} \tfrac{1}{2} \langle \phi^2 \rangle = \tfrac{1}{2} k_B T . \tag{C2}$$

The existence of a probability distribution $P(\phi)$ reduces the maximum potential energy that the system can gain by adjusting its average phase to $\langle \phi \rangle = 0$. This reduction can be calculated according to

$$\langle \cos\phi \rangle = \text{Re} \left[\int_{-\infty}^{\infty} d\phi \, P(\phi) e^{i\phi} \right] = e^{-\langle \phi^2 \rangle / 2} . \tag{C3}$$

On this basis, the average depinning field should be reduced by the same factor,

$$e^{-\langle \phi^2 \rangle / 2} = e^{-T/T_0} , \tag{C4}$$

where

$$T_0 = 2 V_{\max} / k_B . \tag{C5}$$

For a pinning potential of the form given in Eq. (6.1), we make the identification

$$V_{\max} \approx \frac{2}{\pi^2} E_{\text{pin}}(\pi) , \tag{C6}$$

which yields the result quoted in Eq. (6.11).

[1] P. Monceau, N. P. Ong, A. M. Portis, A. Meerchaut, and J. Rouxel, Phys. Rev. Lett. **37**, 602 (1976).
[2] R. M. Fleming and C. C. Grimes, Phys. Rev. Lett. **42**, 1423 (1979).
[3] R. M. Fleming, D. E. Moncton, and D. B. McWhan, Phys. Rev. B **18**, 5560 (1978).
[4] R. M. Fleming, Phys. Rev. B **22**, 5606 (1980).
[5] N. P. Ong and P. Monceau, Phys. Rev. B **16**, 3443 (1977).

[6]S. W. Loncor and A. M. Portis, Bull. Am. Phys. Soc. **25**, 340 (1980).
[7]G. Grüner, L. C. Tippie, J. Sanny, W. G. Clark, and N. P. Ong, Phys. Rev. Lett. **45**, 935 (1980).
[8]J. C. Gill, Solid State Commun. **37**, 459 (1981).
[9]G. Grüner, A. Zawadowski, and P. M. Chaikin, Phys. Rev. Lett. **46**, 511 (1981).
[10]P. Monceau, J. Richard, and M. Renard, Phys. Rev. B **25**, 931 (1982).
[11]P. A. Lee and T. M. Rice, Phys. Rev. B **19**, 3970 (1979).
[12]H. Fukuyama and P. A. Lee, Phys. Rev. B **17**, 535 (1978).
[13]John Bardeen, in *Quasi One-Dimensional Conductors I,* Vol. 95 of *Lecture Notes in Physics,* edited by S. Barisic, A. Bjelis, J. R. Cooper, and B. Leontic (Springer-Verlag, Berlin, 1979), p. 3.
[14]John Bardeen, in *Highly Conducting One-Dimensional Solids,* edited by J. T. Devreese, R. P. Evrard, and V. E. Van Doren (Plenum, London, 1979), p. 373.
[15]H. Fröhlich, Proc. R. Soc. London, Ser. A **223**, 296 (1954).
[16]John Bardeen, Phys. Rev. Lett. **42**, 1498 (1979).
[17]John Bardeen, Phys. Rev. Lett. **45**, 1978 (1980).
[18]J. R. Tucker, IEEE J. Quantum Electron. **QE-15**, 1234 (1979).
[19]J. H. Miller, Jr., J. Richard, J. R. Tucker, and John Bardeen, Phys. Rev. Lett. **51**, 1592 (1983).
[20]J. H. Miller, Jr., R. E. Thorne, W. G. Lyons, J. R. Tucker, and John Bardeen, Phys. Rev. B **31**, 5229 (1985).
[21]L. Sneddon, M. C. Cross, and D. S. Fisher, Phys. Rev. Lett. **49**, 292 (1982).
[22]R. A. Klemm and J. R. Schrieffer, Phys. Rev. Lett. **51**, 47 (1983).
[23]D. S. Fisher, Phys. Rev. Lett. **50**, 1486 (1983); Phys. Rev. B **31**, 1396 (1985).
[24]L. Sneddon, Phys. Rev. B **29**, 719 (1984); **29**, 725 (1984).
[25]P. B. Littlewood, Phys. Rev. B **33**, 6694 (1986).
[26]S. N. Coppersmith and P. B. Littlewood, Phys. Rev. Lett. **57**, 1927 (1986).
[27]P. Monceau, J. Richard, and M. Renard, Phys. Rev. Lett. **45**, 43 (1980).
[28]A. Zettl and G. Grüner, Phys. Rev. B **29**, 755 (1984).
[29]R. P. Hall and A. Zettl, Phys. Rev. B **30**, 2279 (1984).
[30]R. E. Thorne, W. G. Lyons, J. W. Lyding, J. R. Tucker, and John Bardeen, Phys. Rev. B **35**, 6348 (1987); **35**, 6360 (1987).
[31]R. E. Thorne, J. R. Tucker, and John Bardeen, Phys. Rev. Lett. **58**, 828 (1987).
[32]G. Grüner and A. Zettl, Phys. Rep. **119**, 117 (1985).
[33]P. Monceau, in *Electronic Properties of Inorganic Quasi-One-Dimensional Compounds,* edited by P. Monceau (Reidel, Dordrecht, 1985), Pt. II, p. 139.
[34]D. Reagor, S. Sridhar, and G. Grüner, Phys. Rev. B **34**, 2212 (1986).
[35]S. Sridhar, D. Reagor, and G. Grüner, Phys. Rev. B **34**, 2223 (1986).
[36]D. Reagor, S. Sridhar, M. Maki, and G. Grüner, Phys. Rev. B **32**, 8445 (1985).
[37]J. D. Kulick and J. C. Scott, Solid State Commun. **32**, 217 (1979).
[38]G. Grüner and A. Zettl, Phys. Rep. **119**, 129 (1985).
[39]T. Takagaki, M. Ido, and T. Sambongi, J. Phys. Soc. Jpn. Lett. **45**, 2039 (1978).
[40]K. K. Fung and J. W. Steeds, Phys. Rev. Lett. **45**, 1696 (1980).
[41]Use of the estimates given in Sec. II includes an additional factor of $(2/\pi)^2$. Here we adopt the exact value for K that is derived in one-dimensional models.
[42]P. A. Lee, T. M. Rice, and P. W. Anderson, Solid State Commun. **14**, 703 (1974).
[43]G. Grüner and A. Zettl, Phys. Rep. **119**, 155 (1985).
[44]J. H. Ross, Jr., Z. Wang, and C. P. Slichter, Phys. Rev. Lett. **56**, 663 (1986).
[45]W.-Y. Wu, A. Janossy, and G. Grüner, Solid State Commun. **49**, 1013 (1984).
[46]D. Reagor and G. Grüner, Phys. Rev. Lett. **56**, 659 (1986).
[47]J. R. Tucker, W. G. Lyons, J. H. Miller, Jr., R. E. Thorne, and J. W. Lyding, Phys. Rev. B **34**, 9038 (1986).
[48]R. J. Cava, P. Littlewood, R. M. Fleming, R. G. Dunn, and E. A. Rietman, Phys. Rev. B **33**, 2439 (1986).
[49]R. J. Cava, R. M. Fleming, P. Littlewood, E. A. Rietman, L. F. Schneemeyer, and R. G. Dunn, Phys. Rev. B **30**, 3228 (1984).
[50]R. J. Cava, R. M. Fleming, R. G. Dunn, and E. A. Rietman, Phys. Rev. B **31**, 8325 (1985).
[51]The experimental values for $\varepsilon(\omega\rightarrow 0)$ given in Refs. 49, 50, and 52 must be multiplied by a factor of 4π to correct a normalization error.
[52]R. J. Cava, L. F. Schneemeyer, R. M. Fleming, P. B. Littlewood, and E. A. Rietman, Phys. Rev. B **32**, 4088 (1985).
[53]D. Reagor, T. W. Kim, W. P. Beyermann, and G. Grüner, Bull. Am. Phys. Soc. **32**, 521 (1987).
[54]R. M. Fleming, R. J. Cava, L. F. Schneemeyer, E. A. Rietman, and R. G. Dunn, Phys. Rev. B **33**, 5450 (1986).
[55]H. K. Ng, G. A. Thomas, and L. F. Schneemeyer, Phys. Rev. B **33**, 8755 (1986).
[56]R. M. Fleming, L. F. Schneemeyer, and D. E. Moncton, Phys. Rev. B **31**, 899 (1985).
[57]Z. Z. Wang, H. Salva, P. Monceau, M. Renard, C. Roucau, R. Ayroles, F. Levy, L. Guemas, and A. Meerchaut, J. Phys. (Paris) Lett. **44**, L311 (1983); C. Roucau, J. Phys. (Paris) Colloq. **44**, C3-1725 (1983).
[58]G. Grüner, Physica B + C **143B**, 8 (1986).
[59]K. Maki, Phys. Rev. B **33**, 2852 (1986).
[60]A. M. Portis, Mol. Cryst. Liq. Cryst. **81**, 59 (1982).
[61]R. E. Thorne, J. H. Miller, Jr., W. G. Lyons, J. W. Lyding, and J. R. Tucker, Phys. Rev. Lett. **55**, 1006 (1985).
[62]Joseph H. Ross, Jr., Ph.D. thesis, University of Illinois at Urbana-Champaign, 1986 (unpublished).
[63]See Ref. 62, pp. 99 and 100.
[64]A. Janossy, C. Berthier, P. Segransan, and P. Butaud, Phys. Rev. Lett. **59**, 2348 (1987).
[65]P. Segransan, A. Janossy, C. Berthier, J. Marcus, and P. Butaud, Phys. Rev. Lett. **56**, 1854 (1986).
[66]D. C. Douglass, L. F. Schneemeyer, and S. E. Spengler, Phys. Rev. B **32**, 1813 (1985).
[67]R. M. Fleming and L. F. Schneemeyer, Phys. Rev. B **33**, 2930 (1986).
[68]M. Ido, Y. Okajima, H. Wakimoto, and M. Oda, Physica B + C **143B**, 54 (1986).
[69]I. Tütto and A. Zawadowski, Phys. Rev. B **32**, 2449 (1985).
[70]J. W. Brill, N. P. Ong, J. C. Eckert, J. W. Savage, S. K. Khanna, and R. B. Somoano, Phys. Rev. B **23**, 1517 (1981).
[71]S. Liu and L. Sneddon, Phys. Rev. B **35**, 7745 (1987).
[72]P. Monceau, in *Electronic Properties of Inorganic Quasi-One-Dimensional Compounds,* Ref. 33, p. 164.
[73]B. Horovitz, H. Gutfreund, and M. Weger, Phys. Rev. B **12**, 3174 (1975).
[74]K. Carneiro, in *Electronic Properties of Inorganic Quasi-One-Dimensional Compounds,* Ref. 33, Pt. II, p. 1.